ITRI

GASEOUS RADIATION IN HYPERSONIC STAGNATION POINT FLOW

IITRI Project N6011

Office of Naval Research
Washington 25, D.C.

IIT RESEARCH INSTITUTE
Technology Center
Chicago 16, Illinois

GASEOUS RADIATION IN HYPERSONIC STAGNATION POINT FLOW

Final Report

IITRI Project No. N-6011
Contract No. NONR 3884(00)

by

Imants Reba

for

Department of the Navy
Office of Naval Research
Washington 25, D.C.

This work has been sponsored by the Advanced Research Projects Agency (Ballistic Missile Defense Office) and technically administered by the Fluid Dynamics Branch of the Office of Naval Research.

July, 1964

FOREWORD

This is the final report for Contract No. Nonr-3884(00), ARPA order number 322-62. The program was sponsored by the Advanced Research Projects Agency and monitored by the Office of Naval Research with Morton Cooper, the project technical monitor.

The author gratefully acknowledges the assistance of the following persons:

L. N. Wilson and D. S. Hacker, who initiated this program; Mark Cann for his assistance in the interpretation of spectrographic data and Edward Wolthausen for his invaluable help in the experiments.

Respectfully submitted,

IIT RESEARCH INSTITUTE

Imants Reba
Project Engineer

APPROVED:

W. J. Christian, Manager
Heat and Mass Transfer

I. B. Fieldhouse, Assistant Director
Fluid Dynamics Division

ABSTRACT

The problem of gaseous radiation in a hypersonic stagnation point flow was investigated. The experiments were performed in a 3-inch diameter buffered shock-tube. The investigation covered the following phases:

1. Photographic study of luminous bow-shock regions
2. Total light radiation measurements
3. Spectral light intensity measurements
4. Spectrographic study of radiating species.

The photographic study yielded information regarding standoff distances in the shock tube flow. These measurements have been correlated with various theoretical predictions.

The light intensity measurements were made at the stagnation point of two hemisphere cylinders 3/8 inch and 3/4 inch in diameter. These measurements were made using a glass fiber light tube. The underlying philosophy of this program was to develop a technique which would enable us to determine the onset of non-equilibrium in shock tube flows as a function of the initial pressure and the temperature at the stagnation point. The test results discussed in this paper indicate that light intensity measurements made with two models of different characteristic dimensions can be used successfully to obtain this information. With such information at hand the light intensity measurements were made at three flow regimes for the wavelength region between 3700 A and 6300 A:

1. Equilibrium flow (initial pressure 1mm Hg, T_s, 6200°K)
2. Non-equilibrium flow (initial pressure .15mm Hg, T_s, 6200°K)
3. Advanced non-equilibrium flow (initial pressure .1mm Hg T_s, 6200°K).

The spectral light intensity measurements obtained in an equilibrium flow have been used to estimate the radiant heat flux to re-entering vehicles. These measurements are compared with predictions made by other investigators.

Fair agreement is obtained at 1mm Hg initial pressure. Large deviations are observed in comparison with theoretical predictions for equilibrium flow at .1mm Hg.

Spectrographic study yields information about predominant air and impurity radiators in the spectral region from 2000 A to 6500 A. This information was obtained by transverse viewing of the bow shock region as well as viewing through the stagnation point. The results indicate that measurements made through the stagnation point minimize but do not eliminate impurity (particularly CN) contributions to radiation.

TABLE OF CONTENTS

LIST OF ILLUSTRATIONS

LIST OF TABLES

I. INTRODUCTION

Measurement of gaseous radiation to which vehicles are exposed during hypersonic flight presents many problems. On the other hand, radiation measurements in the laboratory also present difficulties, since true flight conditions are difficult to simulate. In the past, attempts have been made to predict the equilibrium or nonequilibrium radiation using the results obtained from measurements of emission behind the normal or reflected shock waves produced in shock tubes. Application of these results to predictions of radiant heating under inflight conditions has been inexact for two reasons. Firstly, the predictions necessarily have been based on approximate descriptions of conditions within the shock layer. Secondly, the radiation measurements made across the shock tube may not truly represent the radiation incident upon the model, since radiation from impurities in the wall boundary layer may contribute. In addition, there is uncertainty about the range of flow regimes in which reentry can be simulated in a shock tube. Specifically, measurements of gaseous radiation in shock-tube flows can be used to predict the radiant heat transfer to an actual vehicle if the flow is in equilibrium and the actual temperatures and densities are duplicated. Under such conditions, the body geometry and size are the governing factors in scaling model results. Where the shock-tube flow is not in

equilibrium, scaling of results is difficult, if not impossible. Consequently, we must determine the relationships between test parameters, such as pressure and temperature, which define the limits of flow regimes in a shock-tube test where data are directly applicable to problems of reentry.

Although the problem of light radiation has been studied extensively by a number of investigators,[1,2,3,4,5] our approach to this problem is quite different. Light radiating from the bow shock region is collected by a light tube extending to the stagnation point of the model. This technique constitutes a direct measurement of radiant flux at the stagnation point. Also, impurity radiation originating at the shock-tube wall is excluded from the measurement. As evidenced by the test results, this technique yields good data reproducibility.

Furthermore, as discussed in this report, measurements made with models of two different nose radii enable qualitative reconstruction of radiation intensity profiles in the bow shock region. Consequently, the assessment of the extent of flow equilibrium or nonequilibrium can be made. To obtain the necessary insight into the problem, the study comprised the following phases:

1). Photographic study of the luminous bow shock region over a range of flow regimes.

2). Measurements of total light radiation at the stagnation point.

3). Spectral light intensity measurements at equilibrium and nonequilibrium flow conditions.

4). Spectrographic investigation to identify predominant radiators.

II. EXPERIMENTAL FACILITY AND TECHNIQUES

The experimental studies were made in a 3-inch buffered shock tube using 3/8-inch and 3/4-inch diameter hemisphere-cylinders. The shock tube facility is shown in Figure 1. Experience has shown that a buffered shock tube with argon as the buffer gas can be used advantageously to generate high shock Mach numbers.[6] However, in gaseous radiation studies, our argon buffer tends to produce considerable inconsistencies in light intensity levels, a result of the very diffuse argon-air contact interface. To eliminate all possible causes of data scatter a dry air buffer was substituted for argon in this investigation. In addition, particular care was exercised in shock-tube preparation. Driver contamination was reduced by thorough cleansing of the tube with a sequence of ethanol rinses after each run. The effects of tube-cleaning procedures upon test data are discussed in Section III. After the thanol rinses, the tube was flushed repeatedly with dry air, and then out-gassed at 1-micron pressure. To ensure that the contamination level was the same for each run and that the out-gassing process was essentially complete, the tube was filled with dry air up to 20-microns pressure, evacuated to 1-micron pressure, and the required pumping time recorded. The process was repeated until no further reduction in pumping time was observed. With this method, the tube leak rates were approximately

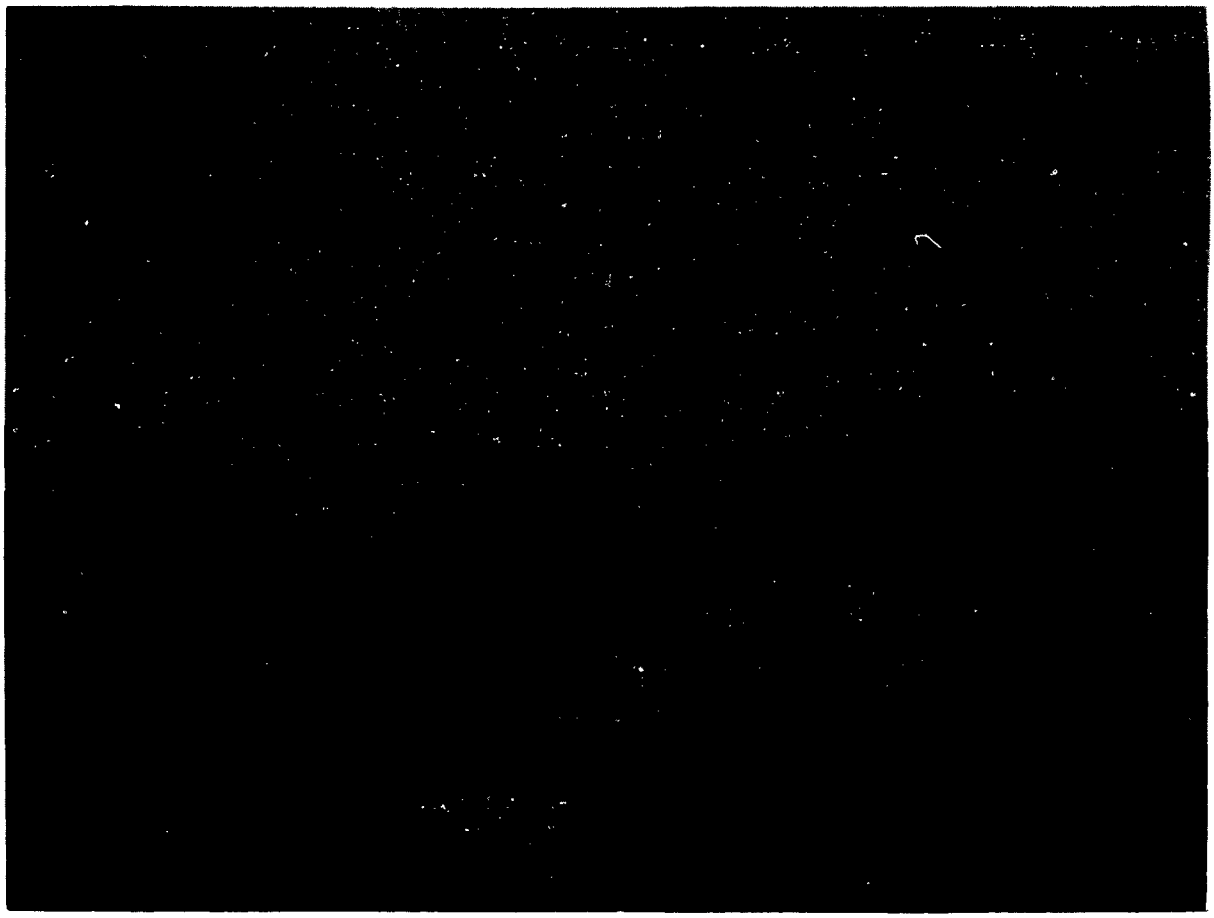

Fig. 1 IITRI 3 INCH BUFFER SHOCK TUBE FACILITY

10 microns per hour. This technique proved to be effective in attaining good data reproducibility. The only departures from these rules were made for total radiation measurements. To reduce the out-gassing time the shock tube was evacuated to 5 microns pressure, then flushed successively.

Initial pressures in the shock tube were monitored by two Alphatron pressure gages which were factory calibrated before this phase of investigation. The shock Mach number was monitored at two photomultiplier stations located 28 inches apart, immediately upstream of the test section. Photomultiplier signals were used to trigger and stop a Beckman counter. Simultaneously, signals were recorded on a Tektronix-555 oscilloscope. With this method, permanent records of shock velocity are obtained. Thus, any counter error resulting from variations in trigger and stopping sensitivity and signal rise-time characteristics can be alleviated.

Radiation measurements were made at the stagnation point of the 3/8-inch and 3/4-inch hemisphere-cylinders (Figure 2). The tips of both models were equipped with profiled opal glass windows to avoid aerodynamic disturbances. Through a passage in the model, a 3mm diameter glass fiber bundle, encased in a Thermofax tubing, extended to the window. The opal glass window is necessary to attain light diffusion and, hence, good angular response characteristics. For total radiation measurements, the collected light was piped through the L-shaped light tube extending through the shock-tube wall directly into a 1P-28 photomultiplier tube. A Ferrand-Uvis monochromator was used between the light

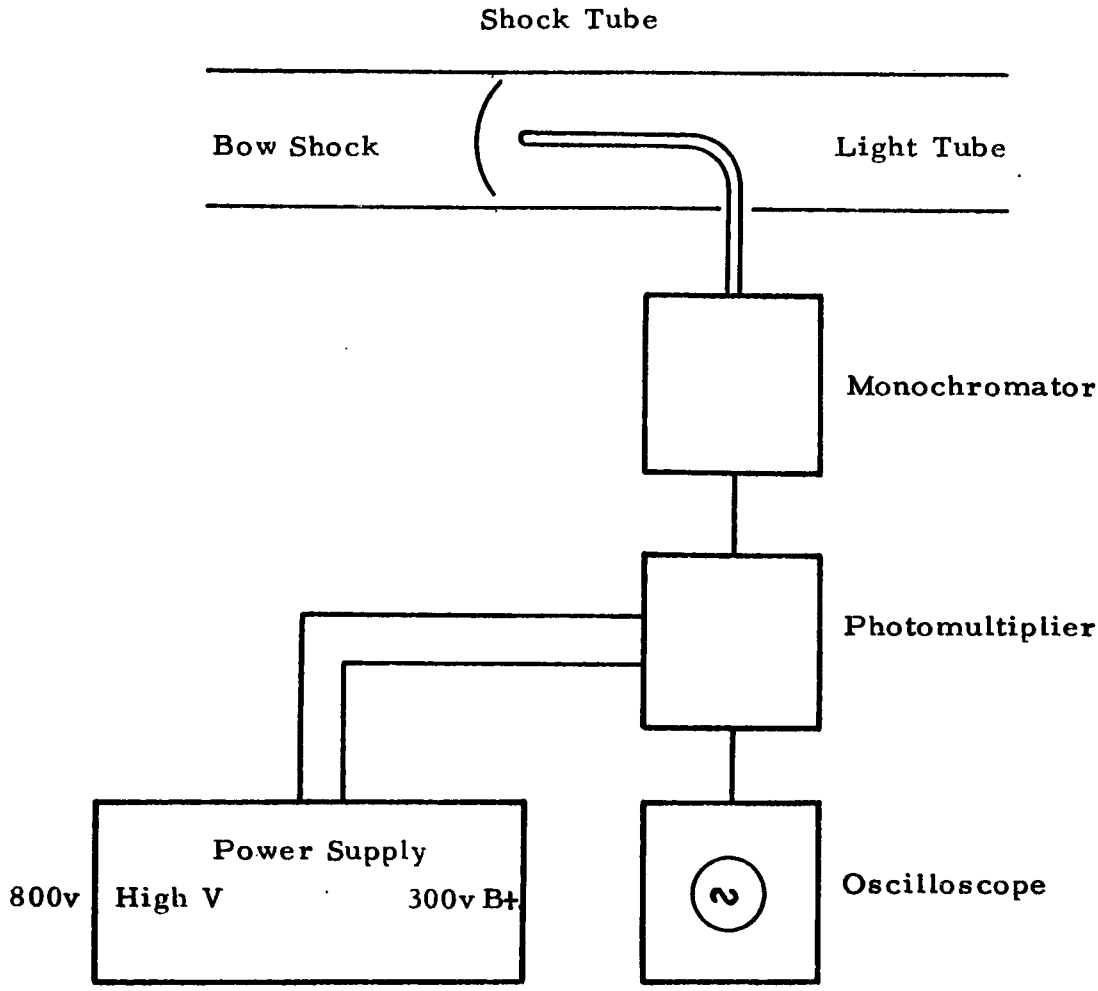

Fig. 2 OPTICAL SYSTEM TO MEASURE RADIANT HEAT TRANSFER AT THE STAGNATION POINT OF A BLUNT BODY

tube output and the 1P-28 photomultiplier tube for spectral measurements. The output from the photomultiplier was recorded on the Tektronix-555 oscilloscope.

In all of the experiments, attempts were made to make the measurements within the linear range of photomultiplier circuitry. In cases where the light output was higher than expected but still below saturation level, data were corrected for any nonlinearities.

For spectrographic studies, a periscope-type system was devised, and the model was provided with a quartz window at the stagnation point. The incoming light rays were bent 90° using a mirror, then focused on the spectrograph entrance slit. The distances between various optical elements of the system and the focal length at the focusing quartz lens were chosen to match the acceptance angle of the spectrograph. In this scheme, the light acceptance angle at the stagnation point was quite small; hence, such a system could not be used for the light intensity measurements. On the other hand, it proved more convenient for spectrographic studies than the use of quartz fiber light tube which was subject to frequent breakage and considerably larger reflection losses.

For the light tube to pick up all radiation incident upon the stagnation point of the model, the angular sensitivity of the light tube should vary as the cosine of the angle of incidence. The angular sensitivity calibrations were performed using collimated light. Tests indicated that angular sensitivity can be modulated by changing the light diffusion characteristics at the

receiving end. This can be accomplished by a single opal glass window approximately 0.030-inch thick, or by a window made out of several layers of flushed-opal glass. The second method seems more favorable since light diffusion can be attained with a smaller reduction in light transmission. Figure 3 compares the calibration data with the desired cosine variation. As this figure shows, the agreement was quite good, and the angular sensitivity did not change even after prolonged exposure to the shock environment.

To establish calibration constants for the light intensity measurements, the complete light-tube system was calibrated by comparison with the calculated intensities from a standard tungsten filament lamp. In this set-up, a quartz lens was used to transpose the image of the tungsten lamp filament through an aperture to the receiving end of the light tube. Therefore, with a one-to-one magnification, the intensity of the filament is very nearly the same as the intensity of the image. For the measurements of the integrated light radiation, the light output was passed directly into a 1P-28 photomultiplier tube. It should be noted that the output obtained in such a manner does not represent the total radiative flux, since the radiative flux is a function of wavelength, as shown in equations 1 and 3. However, such output yields a relative measure of light intensity at a particular flow condition (density and temperature) obtained at the stagnation points of models with different nose radii. Consequently, since the ultimate goal was to establish the intensity ratio for a given flow condition obtained from two models

of different sizes, the calibration procedure is very simple. The light output from a standard tungsten filament lamp was passed directly into a 1P-28 photomultiplier tube. The voltage output measured by an oscilloscope is the calibration constant, since the shock-tube tests were performed using the same voltages as during the calibration. By variation of the voltage setting, adjustments in the calibration constant and light radiation signal could be made, to obtain data within the linear portion of the response curve of the photomultiplier.

For the spectral intensity measurements, the calibration procedure was very similar. Here, however, the output from the light tube was passed first through a monochromator having 0.5mm (100-A total band width) entrance and exit slits, and then into a 1P-28 photomultiplier tube. The calibration was performed over the spectral range from 3700 to 6300A at the wavelengths to be investigated in the experiments. A calibration was performed prior to each run to compensate for any changes in the response characteristics of the light-tube assembly.

The intensity of the tungsten lamp for a given wavelength is given by

$$I_{(\lambda)} = \frac{\varepsilon}{2\pi} \frac{3.742 \times 10^4}{\lambda^5 (\exp \frac{6.4558}{\lambda} - 1)} \frac{\text{watts}}{\text{cm}^2\text{-}\mu \text{ ster}} \qquad (1)$$

where λ is wavelength in microns and ε is the emissivity of tungsten determined from the de Vos tables[7]. Equation (1) is discussed in detail in Reference 8. From the geometric

arrangement of the calibration set-up, the calibration form factor F_{12} can be established:

$$F_{12} = \frac{A_1}{r^2} \times A_2 \quad cm^2\text{- ster} \tag{2}$$

where A_1 is the area of the aperture, A_2 the area of the lamp filament seen by the light tube, and r the distance between the aperture and the light tube. If $V_{\lambda(c)}$ is the voltage output measured during calibration and $V_{\lambda(t)}$ is the voltage output recorded during a shock tube run, then the radiative flux Q_{RAD} is

$$Q_{RAD} = \frac{I_\lambda F_{12} V_{\lambda(t)}}{V_{\lambda(c)} A_2} \quad \frac{watts}{cm^2} \tag{3}$$

To be consistent, runs were made with the same monochromator and photomultiplier system used for calibration. As for the calibration, the test runs were performed with monochromator slits of 0.5mm covering a spectral band 100A wide. Likewise, the voltages used to excite the photomultiplier tube were the same as used in the calibration. In cases where the light output exceeded the capacity of photomultiplier tube, the exciting voltages were reduced so that the output would fall in the linear range of the photo-multiplier.

In general, the use of a fiber bundle, instead of the solid quartz rod, constitutes a major improvement. Although quartz has better light transmission characteristics than glass fibers, holding the quartz rod in the suspension mounts presents severe difficulties at the higher shock Mach numbers. Shifting of the light tube in the mounts leads to inaccuracies

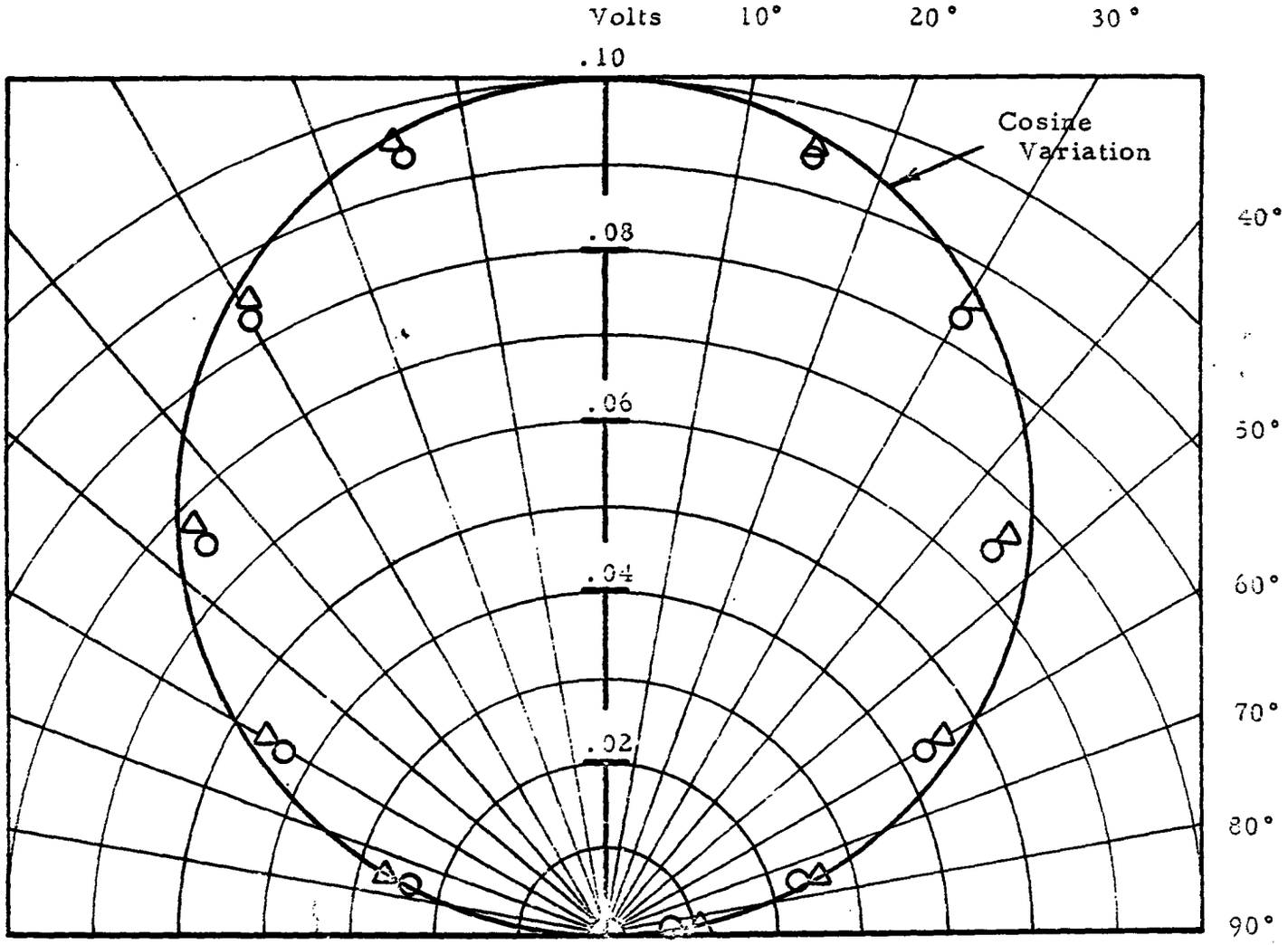

△ Output before shock tube tests

○ Output after 50 shock tube tests

Fig. 3 ANGULAR RESPONSE FOR THE LIGHT TUBE ASSEMBLY USING GLASS FIBER BUNDLE AND OPAL GLASS WINDOW AT THE STAGNATION POINT OF THE MODEL

in test results and ultimately to breakage of the light tube itself. Preliminary measurements using the solid quartz light tube had indicated a radiation level which increased with time throughout the flow duration, even at the highest densities. It appears now that, for the most part, this effect was the result of mechanical changes in the light tube assembly system. The use of a rigidly-mounted fiber bundle avoids this problem. Consequently, any changes in the measured light intensity with time were due to transients in the processes in the bow shock region.

III. DISCUSSION OF RESULTS

1. Photographic Study

Recent examinations of the flow field have shown that predissociation in the free stream can change the standoff distance as well as the bow-shock curvature considerably[9]. At the present time, few experimental data have been collected for such measurements at low density; none, at least, in shock tube flows. Standoff-distance measurements in shock-tube flows provide an experimental verification for various existing theories. Likewise, departures from experimental results indicate that assumptions inherent in these theories are not valid in the flow regime in question. Such knowledge used separately, or in conjunction with the total light-intensity measurements, may constitute an effective means for the evaluation of the predissociation effects and may indicate flow regimes where nonequilibrium is pronounced.

In addition, it yields a measure of the gas volume available for radiation to the surface. Such information is required if radiant heat loads are to be calculated from measurements made behind a normal shock. Consequently, attempts were made to develop a photographic technique that could be applied to flows at very low density.

Conventional flow-visualization techniques such as interferometry, schlieren, and shadowgraph failed to produce the desired results. However, satisfactory results were obtained using direct photography. Typical pictures are shown in Figure 4. To avoid overexposure from reflected waves after the luminous region at the stagnation point of the model had ceased to exist, a shutter that can close within 30 microseconds was constructed. The design and operational characteristics of this shutter are described in Reference 10.

Data were obtained from two hemisphere-cylinders, 3/8 inch and 3/4 inch in diameter. Shock Mach number range was between 10.7 and 14.3 over a range of densities corresponding to initial pressures between 1.5mm Hg and 0.05mm Hg with stagnation temperature of 6200°K. Limitations of light intensity and flow duration did not permit photography at pressures below 0.05mm Hg.

The standoff distance can be determined from mass transfer considerations alone, with the principal variable affecting its value being the density ratio ρ_∞/ρ_s across the shock. The velocity ratio is essentially unaffected by speed dissociation. Experimental values of Δ/R are plotted in

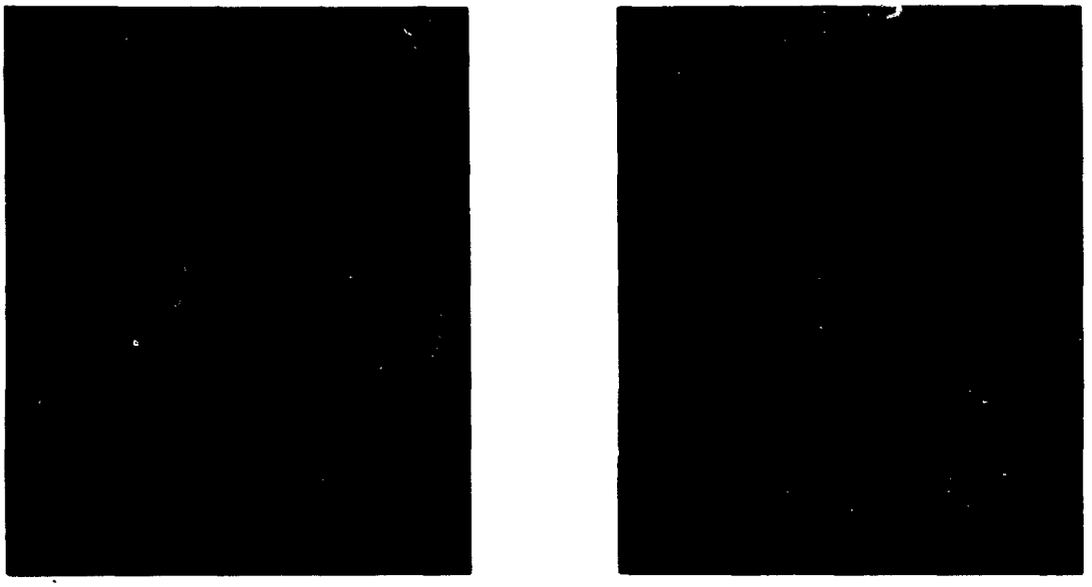

a b

Fig. 4 FORMATION OF BOW SHOCK AT $M_s = 12$

p_1 = 0.5mm Hg, ~ 170 μsec.

a. Model 3/8 inch Dia.

b. Model 3/4 inch Dia.

Figure 5 as functions of the density ratio calculated from Feldman's tables[11] for equilibrium air. The theories of Van Dyke[12] Serbin[13] and others are shown for comparison. At lower Mach numbers and $\rho_2/\rho_3 \cong \rho_\infty/\rho_s$ greater than 0.15, the data correlate well with the Van Dyke analysis. Below $\rho_2/\rho_3 = 0.15$, the disagreement is more pronounced, possibly because of error produced by poorer optical resolution at low densities and nonequilibrium chemistry on either side of the bow shock.

By considering the effect of upstream conditions on flow variables across the shock, it is possible to estimate the directions of the error introduced by the assumption of an equilibrium state for the gas behind the incident normal shock, which produced the flow around the model. As the initial pressure is lowered, there is an accompanying decrease in available test time. This effect has been predicted by Roshko[14] and verified by Hacker and Wilson[15]. Coupled with the decrease in flow duration, chemical relaxation times in the gas become longer; hence, an accurate description of the gas composition and its flow properties is difficult to establish. Even at higher densities ($p_1 > 0.1$mm Hg), the flow about the body is still uncertain since the free stream has been heated and dissociated ahead of the bow shock. Inger[9] has described a model for the stagnation region in the presence of a partially dissociated free stream. Significant increases in shock detachment distance are predicted for increasing levels of dissociation. The free-stream dissociation level also increases the stagnation density ratio.

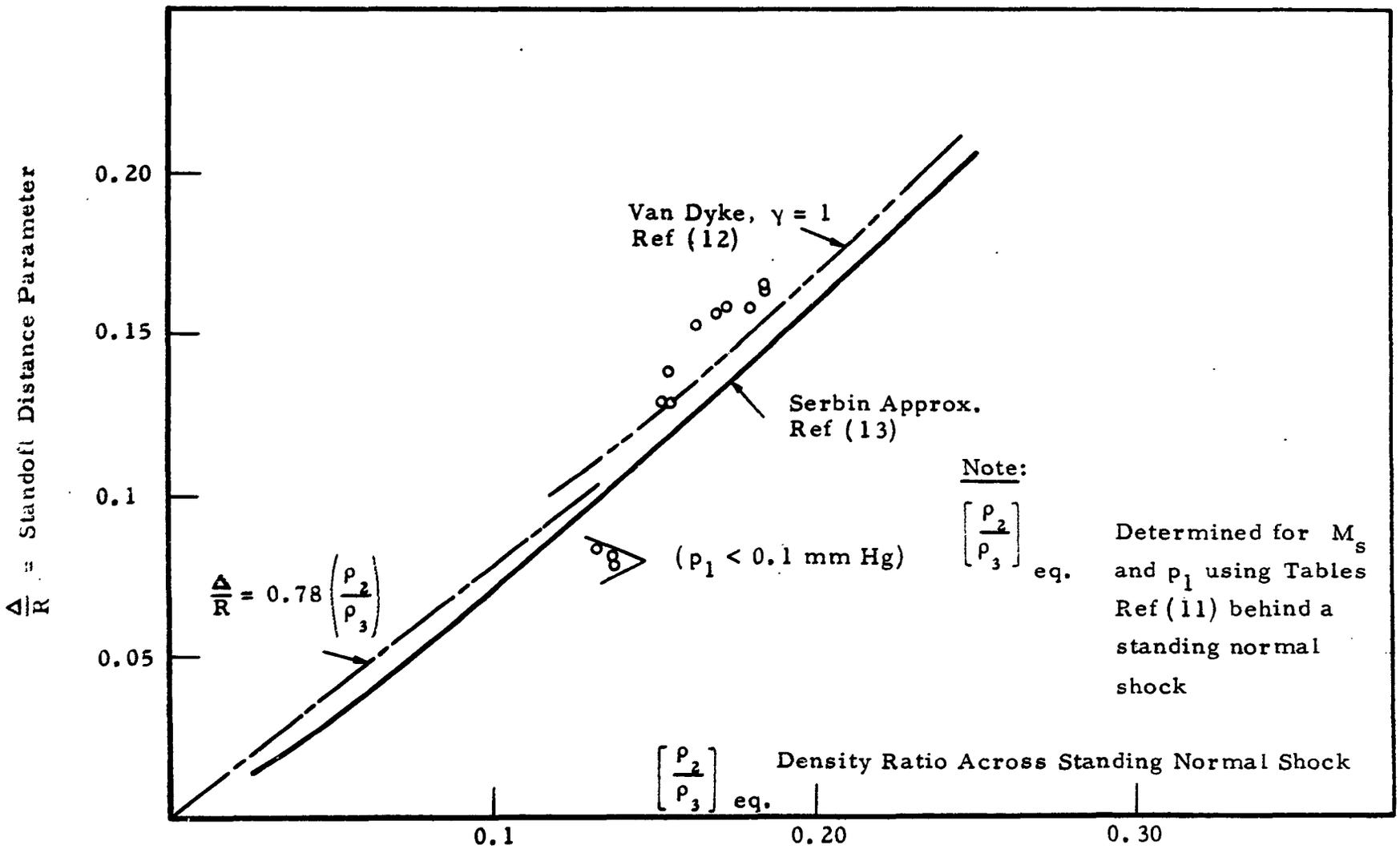

Fig. 5 THEORETICAL AND EXPERIMENTAL RESULTS FOR STANDOFF DISTANCE PARAMETER

These facts suggest the probable reasons for the deviations of the present data from the theoretical values. First, at the higher values of density ρ_2/ρ_3, the measured values of Δ/R are higher than predicted by theory. However, because of air dissociation ahead of the bow shock, the density ratio under experiemental conditions must actually have been larger than the values for undissociated air obtained from Reference 11. Correction of the density ratio to include predissociation effects would, therefore, shift the experimental data closer to the Van Dyke solution.

At the lower density ratios, the experimental Δ/R ratios are considerably below the values predicted by theory. If we can accept the fact that an inviscid field exists in the portion of the experimental range examined and if the optical error is assumed constant throughout, then the deviation at the low-density regime may be identified as resulting from possible nonequilibrium gas effects. It is indeed in this regime that the relaxation times become quite long and appreciable nonequilibrium effects occur behind both incident and bow shocks.

It has been shown by Burke and Boyer[16] that the nonequilibrium effects accompanying the expansion of air in the shock tunnel markedly affect the conditions within the shock layer. Their analysis is applicable to the conditions in the shock tube as well. Under conditions where nonequilibrium chemical processes are important in the shock layer, simulation of of actual flight conditions is out of the question. However, at such conditions where the level of predissociation in the external flow is small, as obtained with relatively weak incident

shock waves, it is possible to achieve at least partial simulation in the shock layer at the stagnation stream line. This has been shown in recent experiments[15] where the Mach numbers of less than 14 were used to achieve stagnation heat transfer data at Reynolds numbers as low as 500. For example, at M_s 14 and p_1 = 0.05mm behind a normal shock in air the oxygen is completely dissociated at equilibrium with an atom concentration of 34 per cent. During relaxation processes this value would be lower. The effect of such a concentration of atoms makes any evaluation of the shock layer radiation extremely sensitive to actual conditions in the flow field.

2. Total Light Intensity Measurements (band width is limited by the photomultiplier-light tube system)

If the flow behind the bow shock is in equilibrium, the intensity of light radiation to the stagnation point should vary almost linearly with the shock stand-off distance or proportionally to the model scale.[17] That is, the stagnation region behind the bow shock can be considered as a slab of gas having a uniform light radiation profile.

However, as the density is decreased and the relaxation region becomes appreciable in extent, but is still less than the shock stand-off distance, the nonequilibrium radiation will dominate and will depend only on the relaxation distance and not on the model scale. Still further reduction in density causes the relaxation distance to increase to such an extent that it becomes larger than the shock stand-off distance. In this flow regime, the radiation to the stagnation point become scale-

dependent again. Hence, by comparing the radiation measured using two models of different scale in identical flow fields, it should be possible to determine when nonequilibrium effects become significant. The data presented in this report substantiate these scaling arguments.

To verify this argument and, hence, the experimental results, a very simple analytical model was considered. As an example, the radiation profiles for N_2^+ (1st negative) were calculated, then used to estimate the variation of radiation intensity with model scale as a function of initial pressure with stagnation temperature kept constant. To estimate the radiation profiles, emission calculations by Camm and co-workers[18] were used. These authors also made calculations for the case where the oxygen was 20 per cent dissociated before the shock front and showed that, under these conditions, relaxation was more rapid and gave rise to larger peak radiation intensities. The experimental mixture is somewhat different than in this calculation. Although the temperatures produced behind the bow shock, at the stagnation point, are within 3 per cent of one of the calculated conditions of Camm, et.al,[18] the pressures and also the prehistory of the gas are different. In our experiments, the gas is heated by a normal shock and this compressed, heated gas flows into the bow shock. It was considered desirable to discover whether the nonequilibrium characteristics of the radiation changed over the range of the experimental conditions, these changes being attributable to changing relaxation rates.

For this purpose, the data from Reference 18 were used, making adjustments to the time constants to allow for the different experimental conditions. The results are necessarily very approximate but, even so, they afford an interesting comparison with the data recorded by the light tube-photomultiplier combination.

The nonequilibrium radiation profile can be approximated by the expression:

$$\frac{I}{I_{eq}} = A(e^{-t/\tau_2} - e^{-t/\tau_1}) + (1 - e^{-t/\tau_2}) \qquad (4)$$

where

τ_1 = time constant for rising profile

τ_2 = time constant for falling profile

A = Constant

I_{eq} = Equilibrium radiation intensity

τ_1 and τ_2 were found from the data of Reference 18; the calculation was confined to the N_2^+ (1st negative) profiles, but, as shown in Reference 18, profiles for NO_β would be quite similar, only slightly slower. Time constants were estimated from the published graphs for various shock strengths and plotted as functions of ΔT, where ΔT is the temperature rise across the shock and temperature fall from the shock front to equilibrium, respectively. Time constants were then obtained from curves for the ΔT appropriate to the present experimental conditions. These time constants were then corrected for experimental pressures assuming that binary collisions predominated. Equation 4 together with the appropriate time constants, allows the radiation intensity profile calculation, subject to a value for the constant A,

which determines the peak value for I/I_{eq}.

The work of the Camm group shows this ratio to vary between 7 and 10, therefore, for the present calculation, the value of A was adjusted to yield $(I/I_{eq})_{max}$ 10 for all pressures considered. This procedure overestimates the magnitude of non-equilibrium effects, but not the time relations. Profiles calculated in this manner are shown in Figure 6.

To estimate the radiation intensity variation with model scale an extremely simple model of the flow field around the bodies was considered. The particle paths were drawn in an arbitrary manner subject to the continuity requirement. From these paths, the radiation intensity from each point could be estimated and, when corrected for the distance to the receiver, solid angle subtended, and receiver directionality, these calculations yield the total contribution from the gas cap radiation.

The results are as follows:

Initial Pressure (mm Hg)	Light Intensity Ratio $\frac{I_{3/4}}{I_{3/8}}$
1	1.89 (assuming no overshoot)
1	1.61 (with overshoot)
0.15	1.11
0.1	1.95

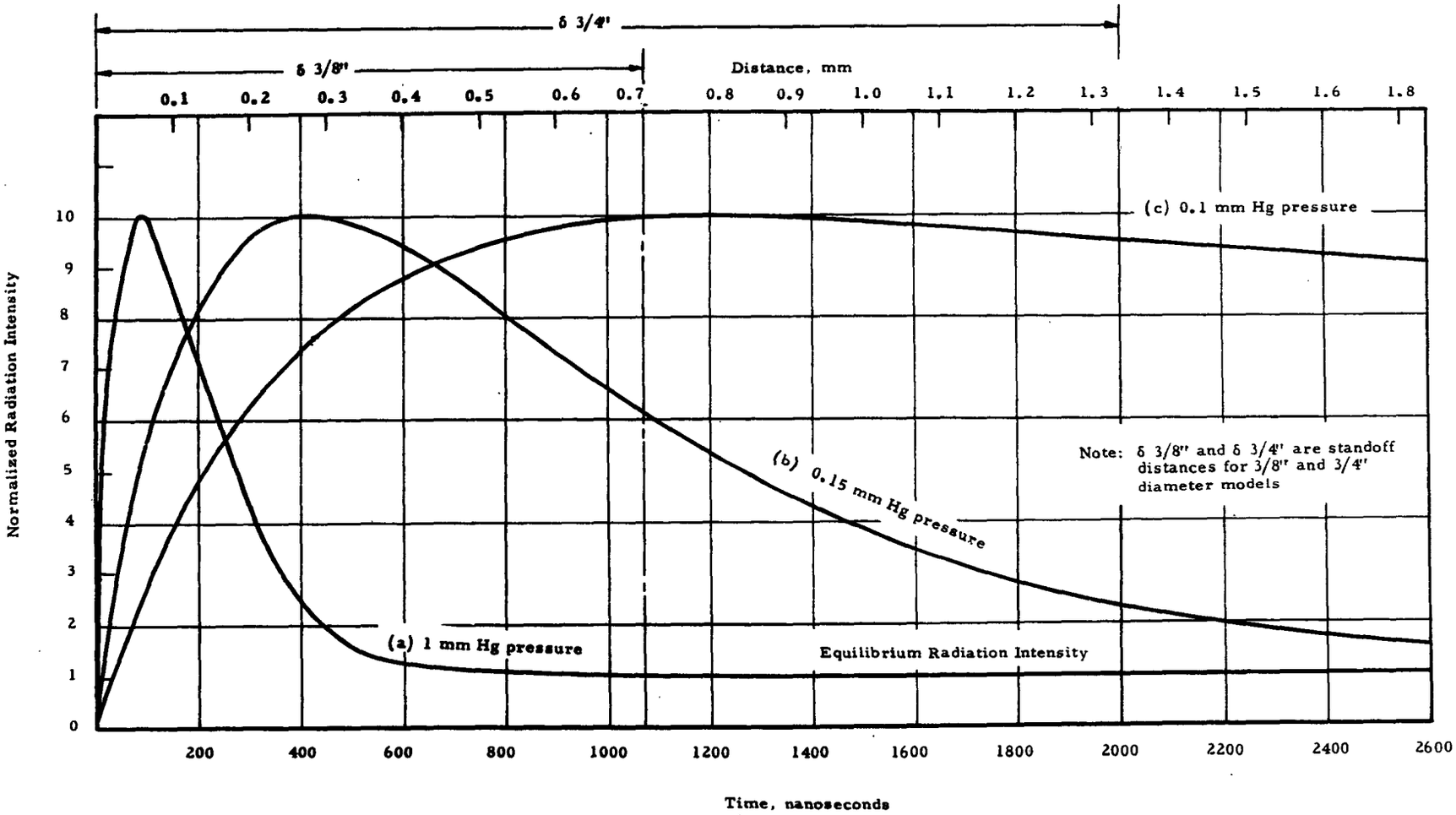

Fig. 6 CALCULATED RADIATION PROFILES FOR N_2^+ (1 st Negative)

Compared with the experimentally obtained values (Figure 7) these ratios indicate considerably larger nonequilibrium effects. This deviation is due to the extremely simple flow field model and to assumptions made in the analysis. As mentioned, the data used from Reference 18 apply to 20 per cent dissociation of oxygen, whereas the estimates of gas composition in the present experiments yield values of approximately 10 per cent for 1mm Hg pressure and 100 per cent for the lower pressures. Hence, the calculated intensity ratios should be used with caution, but do substantiate the interpretation of data. This analysis shows that for the case where nonequilibrium overshoot can be completely neglected, i.e., for a constant radiation profile in the bow shock region, the intensity ratio is 1.89 which is in close agreement with the experimental value. In the flow field model, no allowances were made for changes in temperature overshoot and radiation profiles in the regions away from the stagnation point. In the actual case, the temperature overshoot decreases as the flow passes around the body and, consequently, the relaxation processes are slower.[19]

It is probable that NO-β radiation overshoot was more important than N_2^+ (1st negative). The time profiles in Reference 18 are very similar and, hence, within the accuracy of the present analysis the results can be taken to apply to NO-β also: However, the ratio I/I_{eq} should be rather less. Other transient radiators which, as will be discussed, are very dominant is the spectrograms, are NH, CN, OH; no attempt has been made to calculate these profiles. Analysis which accounts for all these factors and all

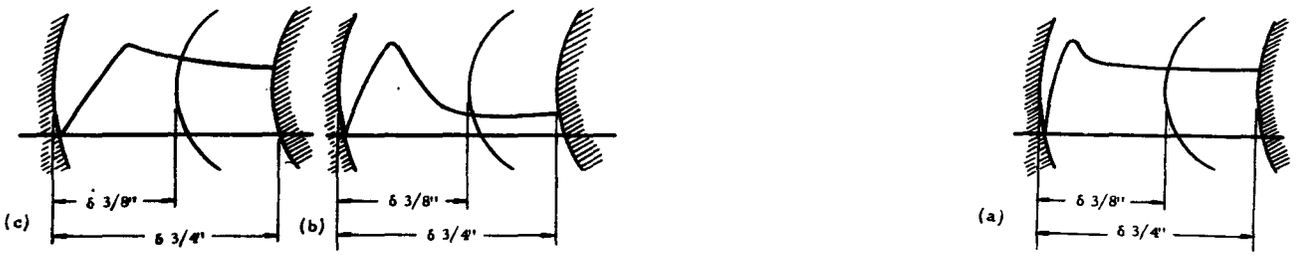

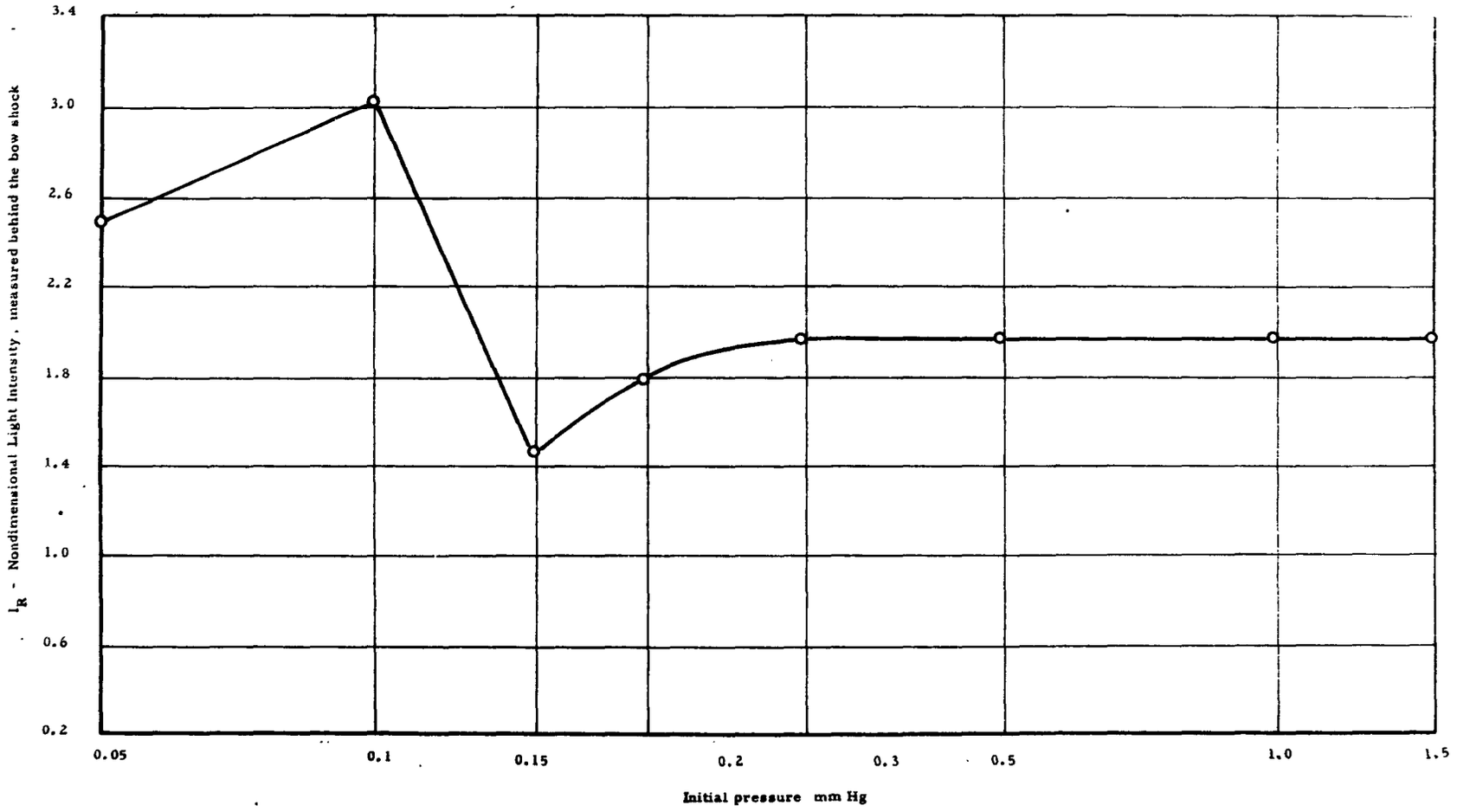

Fig. 7 AVERAGE LIGHT INTENSITY RATIO $I_R = \frac{I_{3/4\text{" dia. model}}}{I_{3/8\text{" dia. model}}}$

The figures (a), (b), and (c) depict the corresponding radiation profiles

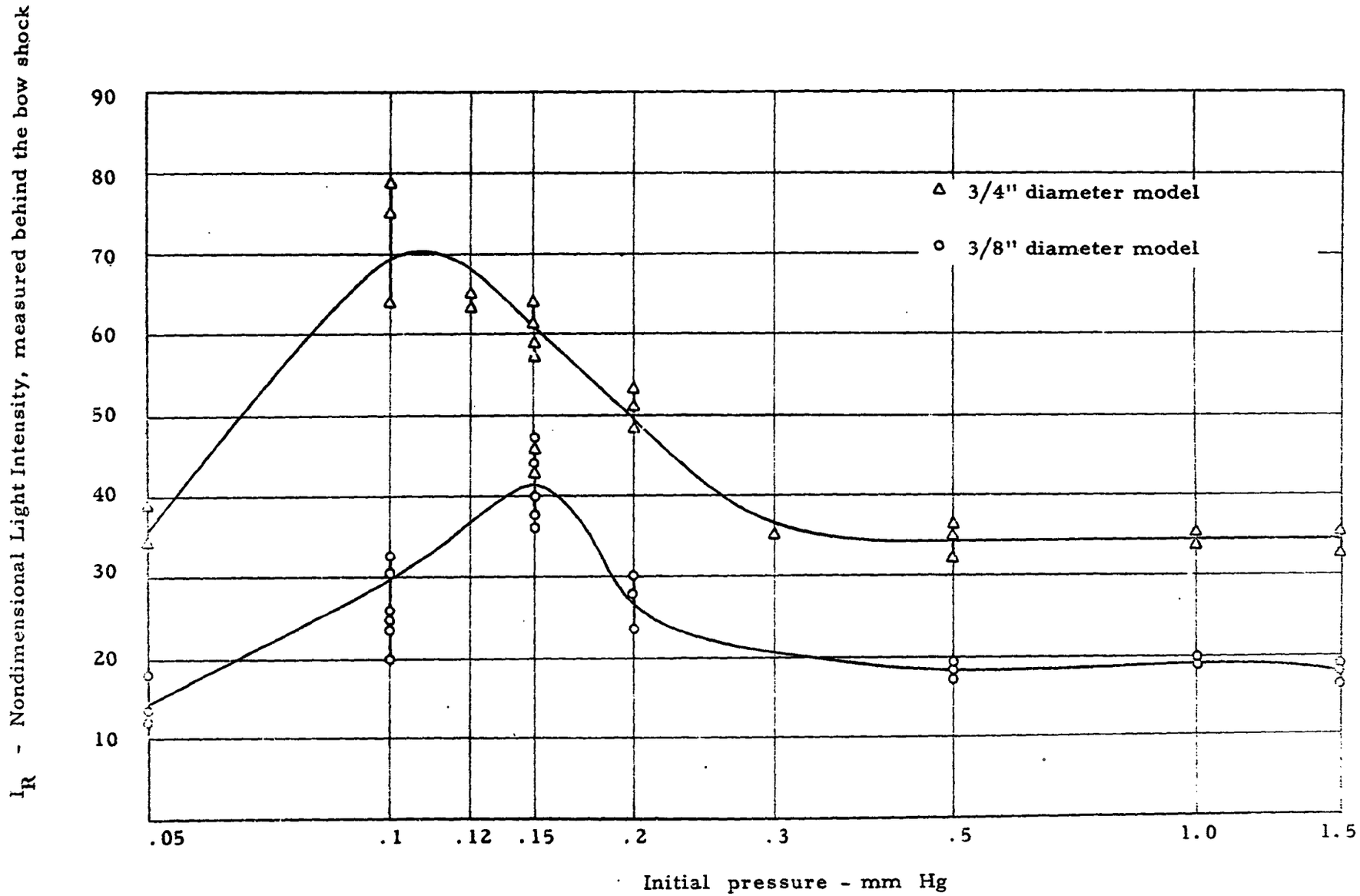

Fig. 8 TOTAL LIGHT INTENSITY MEASUREMENTS

reactions taking place is beyond the scope of this problem. The sole purpose of this analysis is to provide a verification of the postulated interpretation of the light tube measurements.

Total light intensity measurements were made over a range of the initial shock tube pressures with an essentially constant stagnation temperature of 6200°K. The aim of this effort was to investigate the earlier discussed effect of model scale on radiation intensity and, thus, pinpoint flow regimes where spectral intensity measurements should be made. Figures 7 and 8 summarize the results of this investigation. The data were obtained using 3/8-inch and 3/4-inch diameter hemisphere-cylinders, therefore, the model scale factor is very nearly equal to two. Figure 7 shows that the light intensity ratio is very nearly equal to the model scale factor at initial pressures down to 0.3mm Hg; according to the hypothesis, this indicates an essentially constant light radiation profile and flow equilibrium. Lowering the initial pressure but holding the stagnation temperature essentially constant results in deviations of intensity ratio from the scale factor. This, then, suggests the onset of flow nonequilibrium in the bow shock region. The radiation-intensity profiles, which may explain such behavior, are also depicted in Figure 7. The similarity between these profiles and those calculated (Figure 6) is also quite apparent. Another aspect of the radiation character becomes evident if we examine the measured changes in radiation intensity level with pressure (Figure 8) and the calculated radiation profiles for

the three flow regimes (Figure 6). Inspection of the latter indicates that the contribution from nonequilibrium radiation becomes larger with decreasing pressure and exceeds several times the equilibrium value. Furthermore, the extent of standoff distances relative to the relaxation distances implies that, for the 3/8-inch diameter model, essentially equal or even higher radiation intensity levels are expected at 0.15mm Hg pressure than at 0.10mm Hg pressure. This is because at 0.1mm Hg pressure, the intensity is not fully excited during the flow path corresponding to the standoff distance. For the 3/4-inch diameter model the trend is different. Here, at 0.1mm Hg pressure, the relaxation distance is considerably larger than the standoff distance and a considerable portion of the radiating volume gives nonequilibrium radiation which is considerably higher than the equilibrium value. If we consider the calculated radiation profile at 0.15mm Hg pressure, we see that the relaxation process is much faster and, hence, the radiating volume contains less intense radiation. Such trends are evident in measurements shown in Figure 8.

Based on these findings from the total intensity measurements, three flow regimes have been chosen for detailed spectral radiation intensity measurements:

1. Equilibrium regime (Initial pressure, 1mm Hg)
2. Nonequilibrium regime where relaxation distance is smaller than or equal to shock standoff distance (initial pressure, 0.15mm Hg)
3. Advanced nonequilibrium regime where relaxation

distance is larger than shock standoff distance (initial pressure; 0.10mm Hg)

3. Spectral Measurements of Light Intensity

The aim of this investigation was to determine the contribution of radiation to heat transfer rates measured in shock-tube flows as well as to gain detailed insight into radiation characteristics at different flow regimes. At high stagnation enthalphies, heating rates that exceed those predicted by boundary-layer conduction theories have been measured. There have been speculations that this deviation is the result of excessive radiative transfer to the model surface.[20]

The data presented here were obtained at densities corresponding to the initial shock tube pressures of 1, 0.15, and 0.10mm Hg. The shock Mach numbers were adjusted according to equilibrium data[11] to yield equilibrium stagnation temperature of 6200°K. Spectral intensity was measured using a light tube-monochromator-photomultiplier system over the visible portion of the spectrum (3700 to 6400A). The Ferrand monochromator with 0.5mm entrance and exit slits has been used exclusively. The theoretical band-width for this slit size is 110A. Therefore, to ensure full coverage of the region, most of the data has been obtained at 100 A intervals. These data are presented in Figure 9. For both models, as the initial shock-tube pressure is decreased from 1mm to .15 and .1 mm Hg, the radiant flux intensity over the spectral region from 3800 to 4300 A increases considerably. On the other hand, there are relatively smaller

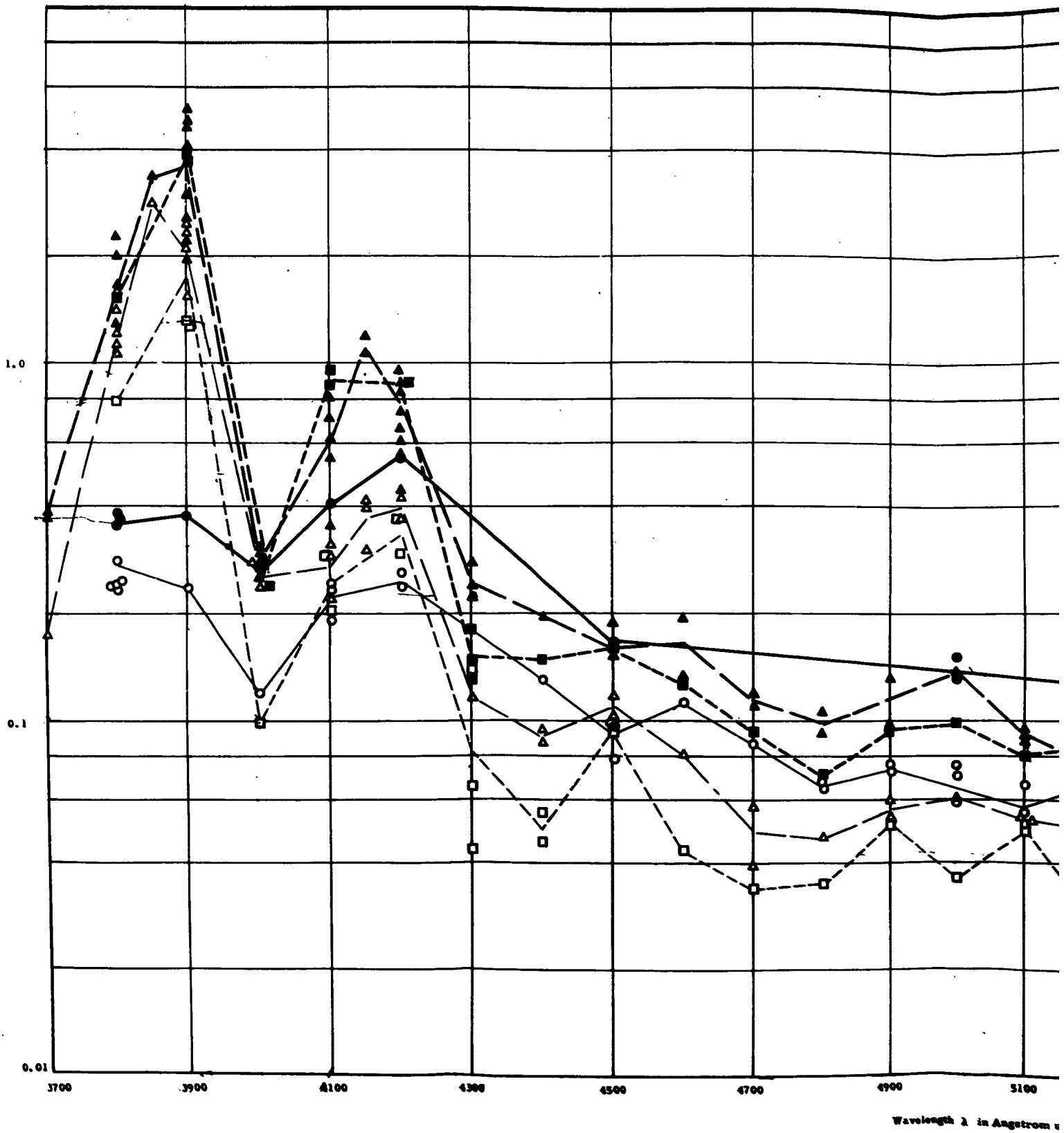

Fig. 9 RADIATIVE HEAT FLUX TO THE STAGNATIO

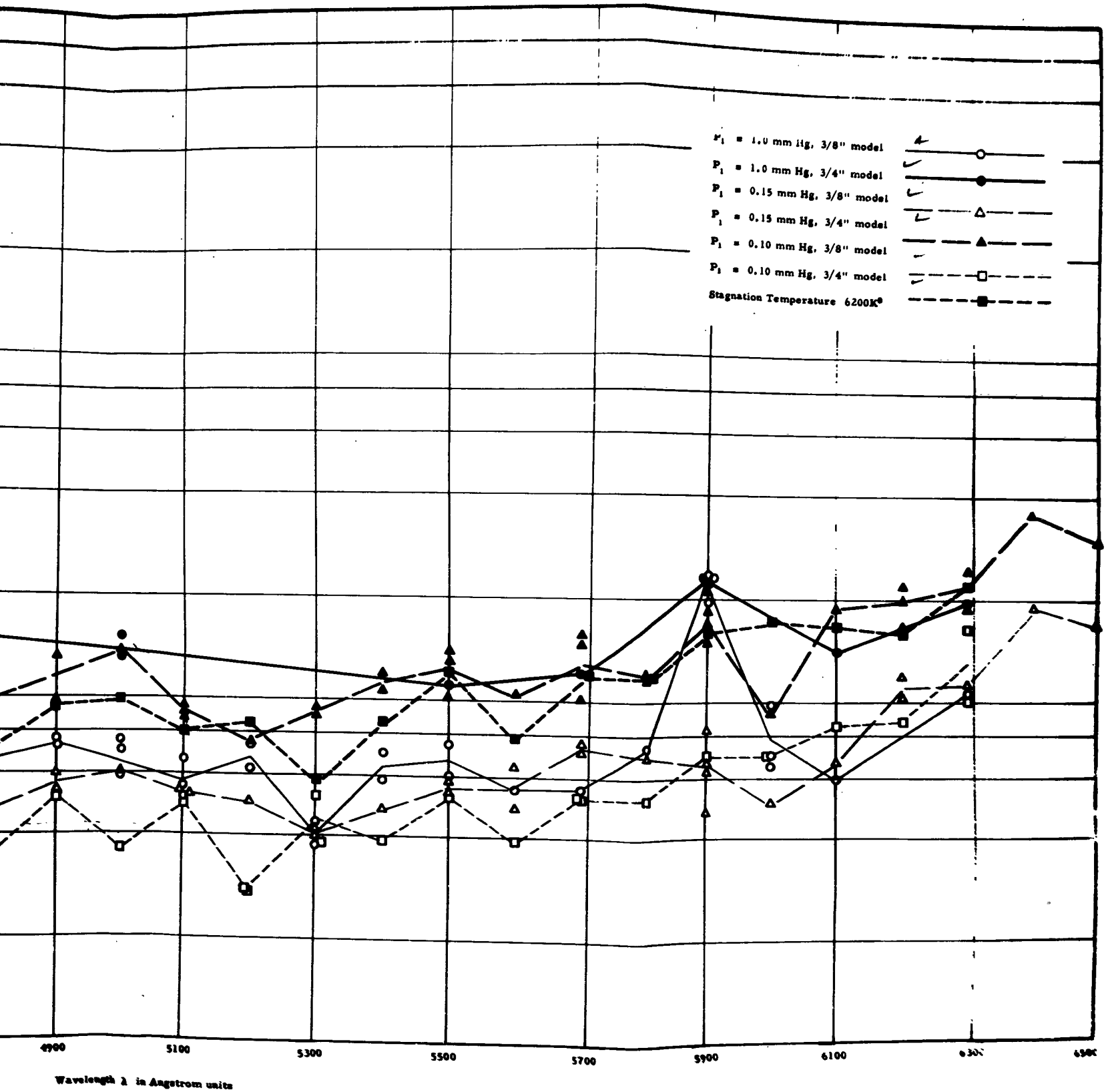

TO THE STAGNATION POINT OF A HEMISPHERE CYLINDER

over-all changes in the intensity level from 4300 to 6300 A. If we consider the criterion for binary scaling, i.e., the intensity level is invariant if ρR is constant where ρ is the density and R the radius of a hemisphere, then for a flow equilibrium, the radiant intensities should be approximately ten times less at 0.1mm Hg than at 1mm Hg for the same model. This condition is not satisfied, hence, here again, particularly in light of the calculated radiation profiles discussed in the preceding section, we can conclude that at lower densities nonequilibrium radiation is observed. This argument is further substantiated by comparison of these data with equilibrium calculations by Breene, et.al. (21) For conversion of data an appropriate view factor I was established by considering the integral:

$$I = \frac{1}{A}\int_{VA}\int\int \frac{\cos\theta}{r^2} \, d\,A\,d\,V \qquad (5)$$

Where A = the area of the receiver

V = the volume of radiating gas

θ = the angle subtended

r = the distance between the receiver and radiating element.

This integral was evaluated graphically, yielding

$$I_{3/4} = 8.82 \quad \frac{mm^3 \ ster}{mm^2}$$ for the 3/4 inch diameter model and

$$I_{3/8} = 4.66 \quad \frac{mm^3 \ ster}{mm^2}$$ for the 3/8 inch diameter model

When the view-factor is used, the radiant flux, given in

$$Q_{RAD} = \frac{\text{watts}}{\text{cm}^2} \quad \text{is changed into}$$

$$Q_{RAD} = \frac{\text{watts}}{\text{cm}^3 \text{ ster}}$$

Data obtained in this investigation are compared with the calculated values of Breene, et.al,[21] in Figures 10 and 11. The 1mm Hg pressure curve in Figure 10 was taken directly from Reference 21. The theoretical curve in Figure 11 was generated by adjusting the contributions from radiating species in accordance with changed equilibrium populations. Here again, the agreement at 1mm Hg pressure is quite good. The only exceptions occur at 5900 and 4200A. As will be discussed, these regions contain strong impurity radiators.

The deviations at 0.1mm Hg pressure, when compared with the equilibrium calculations are quite pronounced (Figure 11). Furthermore, because of deviations from model scale, there is an additional scatter of data points obtained with 3/4-inch and 3/8-inch diameter models. This fact again supports the postulation, that, at pressures below 0.3mm Hg pronounced nonequilibrium prevails.

The integrated radiant flux over the wavelength range is shown in Table 1. These data can be used for heat load predictions.

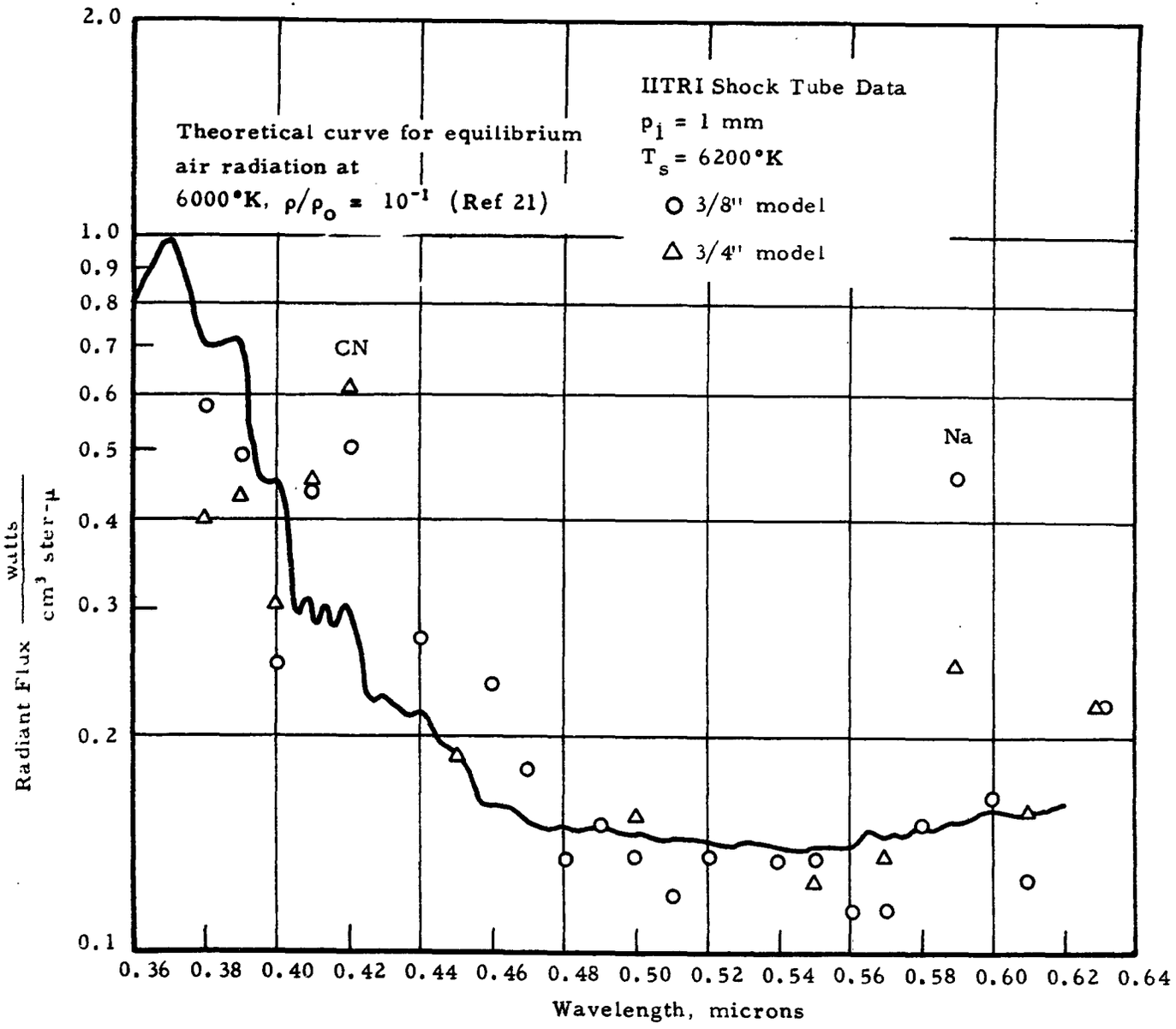

Fig. 10 COMPARISON BETWEEN THE THEORETICAL PREDICTION AND MEASURED RADIANT FLUX AT 1 mm Hg PRESSURE

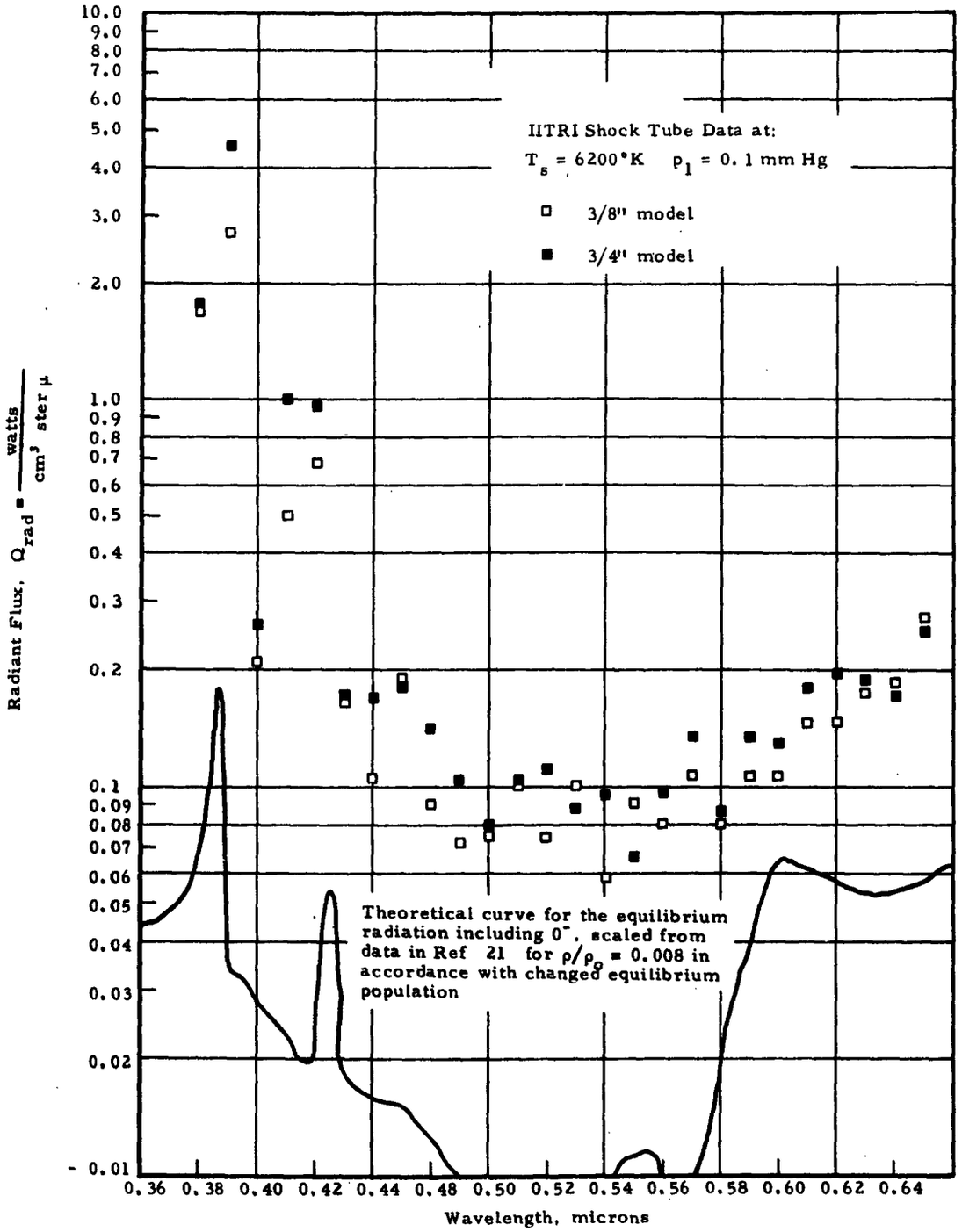

Fig. 11 COMPARISON BETWEEN THE THEORETICAL PREDICTIONS AND MEASURED RADIANT FLUX AT 0.1 mm Hg PRESSURE

Table 1

INTEGRATED RADIANT FLUX

Model Diam (inches)	Initial Pressure (mm Hg)	Q watts/cm^2 (including impurity radiation)
3/4	1.0	50.72×10^{-3}
3/4	0.15	115.70×10^{-3}
3/4	0.10	90.33×10^{-3}
3/8	1.0	26.50×10^{-3}
3/8	0.15	71.14×10^{-3}
3/8	0.10	38.95×10^{-3}

The intensity ratios computed from Table 1 are as follows:

Pressure mm Hg	Intensity Ratio $I_{3/4}/I_{3/8}$
1	1.92
0.15	1.625
0.10	2.22

These values substantiate the scaling arguments which form the basis of this investigation. There is a discrepancy in the value for 0.1mm Hg pressure if comparison is made between the total intensity measurements (Figure 7) and these values. Possibly this is due to the considerable scatter of data at wavelengths around 3900 and 4200 A (Figure 9), which are the predominant contributors to the over-all radiation intensity. Also, as mentioned, total intensity measurements were made at a higher out-gassing pressure, which intensifies impurity radiation, particularly at lower densities. Another factor which becomes evident from these values concerns the heat load prediction from measurements in the shock tube flows. As verified experimentally, at 1mm Hg pressure, essentially equilibrium conditions prevail and the heat load due to radiant heating is proportional to the model scale. For the 3/8-inch diameter model, the Q_{RAD} is 0.0265 watts/cm^2 contributed from air and impurity radiators over the visible portion at the spectrum. The aerodynamic heat transfer, based again on 3/8-inch diameter model at the same flow conditions, was measured[15] to be $Q_{AERO} = 3.18$ kwatts/cm^2. Consequently,

$$Q_{AERO}/Q_{RAD\ (visible)} = 1.2 \times 10^5$$

As shown in the spectrograms and discussed in the following section, at wavelengths below 3700A there is considerable radiation from NO-β, NO-γ, NH, and OH, particularly from the latter two which are impurities. The radiant contributions from these regions were not measured. Also the extent of IR radiation was not measured. However, the absolute level of radiation may be estimated by assuming a very simplified model.

The shocked region at the stagnation point is assumed to radiate as an infinite slab of gas, having a thickness equal to the standoff distance and at the density and temperature equal to the stagnation condition. Further, it is assumed that the gas has a spectrally averaged emissivity per unit length ε, which is dependent upon stagnation temperatures and density. The emissivity of the body surface is unity. With these assumptions the radiant flux is given as:

$$Q_{RAD} = \varepsilon \sigma T^4 \frac{\Delta}{2} \frac{\text{watts}}{\text{cm}^2} \qquad (6)$$

where σ is the Stefan-Boltzmann constant, T is the stagnation temperature, Δ is the shock standoff distance.

The emissivity ε is estimated[22] to be $10^{-3}/\text{cm}$. Likewise, we assume that the standoff distance

$$\Delta \cong RK \qquad (7)$$

where R is the model nose radius and K is the density ratio across the bow shock. Hence with Equations (6) and (7) the total radiant flux for 1mm Hg pressure and a stagnation temperature of 6200°K is

$$Q_{RAD\ (total)} = 0.358\ \text{watts/cm}^2$$

If we compare this value with the aerodynamic heating, we find that

$$\frac{Q_{AERO}}{Q_{RAD\ (total)}} \approx 10^4$$

Since $Q_{RAD} \propto R$ and aerodynamic heating is proportional to $1/R^{1/2}$ then

$$\frac{Q_{AERO}}{Q_{RAD}} \propto \frac{1}{R^{3/2}}$$

Hence, for this particular condition which simulates reentry conditions of approximately 17,000 fps and an altitude of 115,000 ft, Q_{AERO} and Q_{RAD} would be comparable for a body of 210-cm radius.

Another value for $Q_{RAD(total)}$ is obtained from calculations given in Reference 21 for 1mm Hg pressure. As shown in Figure (10) good correlation with the experimental values exists in the spectral region from 3700A to 6300A. The values shown in Table 2 were obtained using appropriate view factors.

Table 2

RADIANT FLUX CALCULATED FROM REFERENCE 21 FOR 1mm Hg PRESSURE

Model Diam (inches)	$\Delta\lambda$ (microns)	Q_{RAD} watts/cm^2
3/8	0.1625 - 0.21	0.03
3/8	0.21 - 0.31	0.10
3/8	0.65 - 0.10	0.0417
3/4	0.1625 - 0.21	0.0556
3/4	0.21 - 0.31	0.185
3/4	0.65 - 0.10	0.0774

These values added to the experimental data yield total radiant heat flux for the 3/8-inch diameter model.

$$Q_{RAD\ (total)} = 0.1985\ watts/cm^2$$

Consequently, the $Q_{RAD\ (total)}$ derived from a simple analysis constitutes a safe upper bound for the flow regime in question.

When attempting to simulate reentry conditions one must simulate given density and temperature conditions for a given flight trajectory and velocity. Since the equilibrium stagnation point conditions are determined by the prescribed reentry, one endeavors to simulate this condition in the laboratory by adjusting the initial shock-tube pressure and shock strength to generate stagnation point conditions. By this means, nonequilibrium densities behind the bow shock similar to those experienced by the reentry vehicle can be reproduced. However, similar non-equilibrium temperature is not produced at the same time.

As a consequence of this inconsistency, the relationship between ρR and Q_{RAD} is not single valued (as it is for equilibrium flow), but depends upon nonequilibrium temperature and its variation which, in turn, changes the reaction rates. Thus, density scaling is no longer applicable.

Here, this applies to flow regimes corresponding to 0.15mm Hg and 0.1mm Hg pressure. Our results show that data depend on model size, however, this dependency is related not only to the characteristic dimension, hence, standoff distance, but is dependent also upon nonequilibrium processes taking place in the bow shock region.

The fact that such deviation can be measured and is in reasonable agreement with a prediction demonstrates the feasibility of this scheme for studies of nonequilibrium radiation. It is quite conceivable that further studies of this kind, carried out over a region of temperatures with density kept constant, would furnish necessary relationships for scaling model test data in nonequilibrium conditions. Although a general scaling cannot be applied, as in a previous case, comparison between the radiant and aerodynamic heat loads for a given model scale can be established from the measurements. Table 3 summarizes these results.

Table 3

COMPARISON, AERODYNAMIC AND RADIANT HEAT FLUX

Model Diam. inches	P mm Hg	Q_{AERO} kwatts/cm^2	Q_{RAD} watts/cm^2	$\frac{Q_{AERO}}{Q_{RAD}}$
3/8	0.15	2.13	0.06396	3.33×10^4
	0.10	1.98	0.03895	5.1×10^4
3/4	0.15	1.52	0.1157	1.31×10^4
	0.10	1.40	0.09033	1.54×10^4

The contributions from UV and IR radiation are not included in the Q_{RAD} values. Even if we assume that such contribution would increase the present value by a factor of ten, the radiant flux as compared with the aerodynamic heating would amount to approximately 0.1 percent. Therefore, deviations in aerodynamic heating measurements[20] cannot be attributed to excessive radiative contributions.

Although the shock tube data obtained at 0.15mm Hg and 0.1mm Hg pressure cannot be applied to the calculation of reentry heating by simple geometric scaling laws, these data enable qualitative analysis of nonequilibrium radiation processes. For this purpose, block diagrams have been computed and are shown in Figure 12. The intensity ratios, given in Figure 12 indicate spectral regions of the most important nonequilibrium radiators. Likewise, it is possible to qualitatively construct an average radiation profile for a particular density. For example, at 0.15mm Hg, the intensity ratios for 50 percent of the points are less than the model scale. This trend indicates that nonequilibrium overshoots exist, as depicted in Figures 6b and 7b. The other half of the points shows that the intensity ratio is greater than the model scale which, in turn, suggests various degrees of advanced nonequilibrium, characterized by the radiation profile in Figure 6c and 7c. Since the radiation level is much higher at lower wavelengths where the intensity ratio is predominantly less than two, the average intensity profile should appear as anticipated from the total radiation measurements at this flow regime (Figure 7b). At 0.1mm Hg pressure, Figure 12c indicates

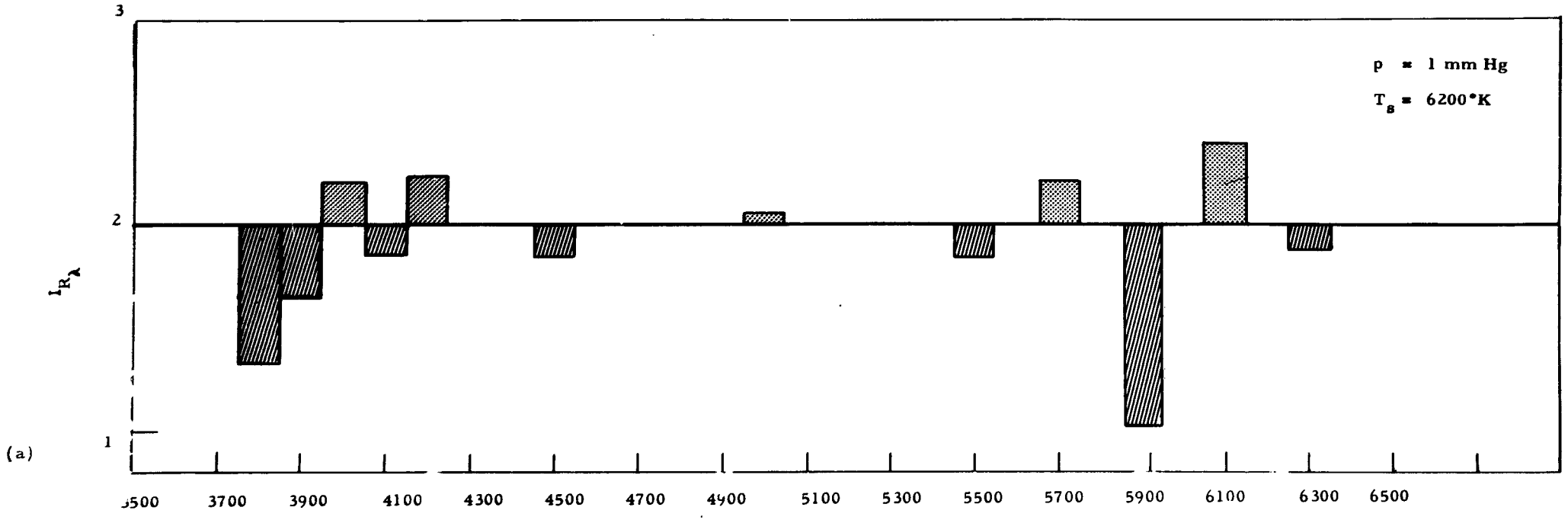
3
2
1
I_{R_λ}
p = 1 mm Hg
T_s = 6200°K
3500
3700
3900
4100
4300
4500
4700
4900
5100
5300
5500
5700
5900
6100
6300
6500

(a)

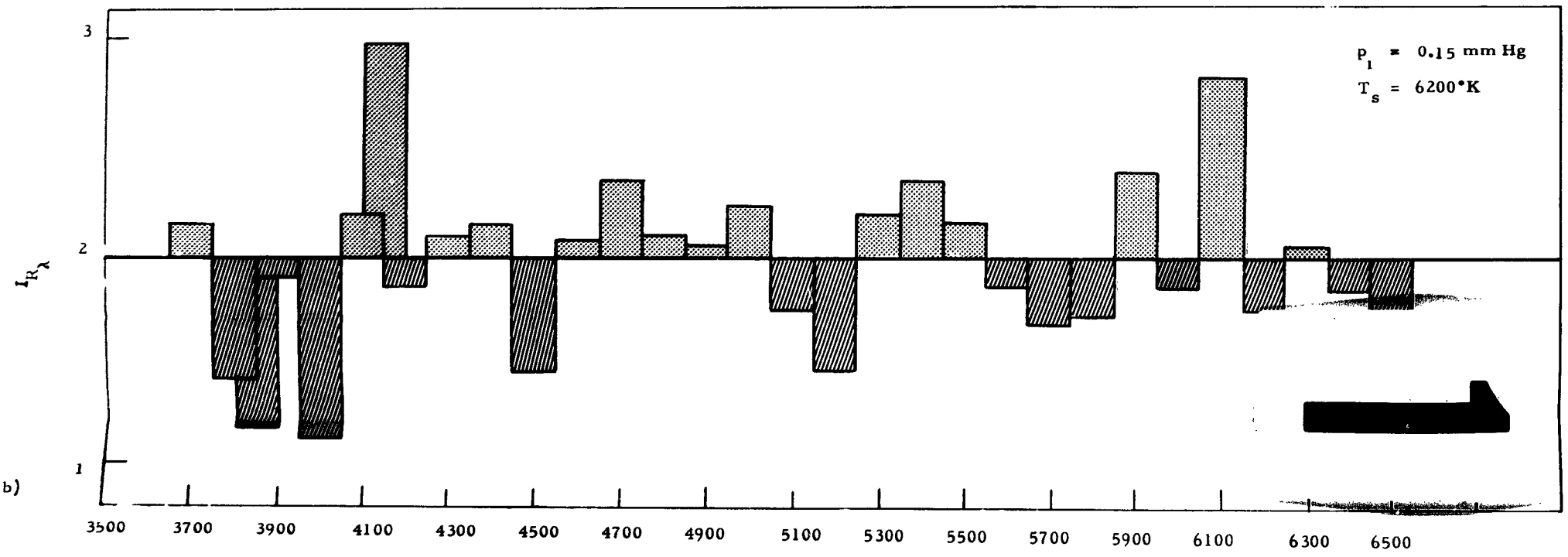
3
2
1
I_{R_λ}
p_1 = 0.15 mm Hg
T_s = 6200°K
3500
3700
3900
4100
4300
4500
4700
4900
5100
5300
5500
5700
5900
6100
6300
6500

(b)

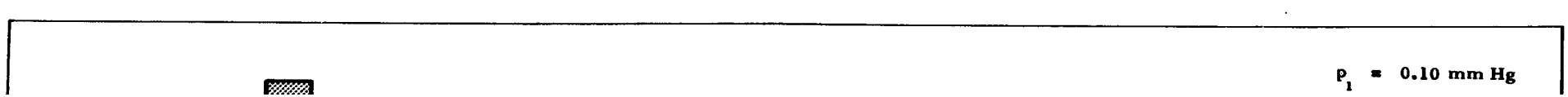
4
p_1 = 0.10 mm Hg

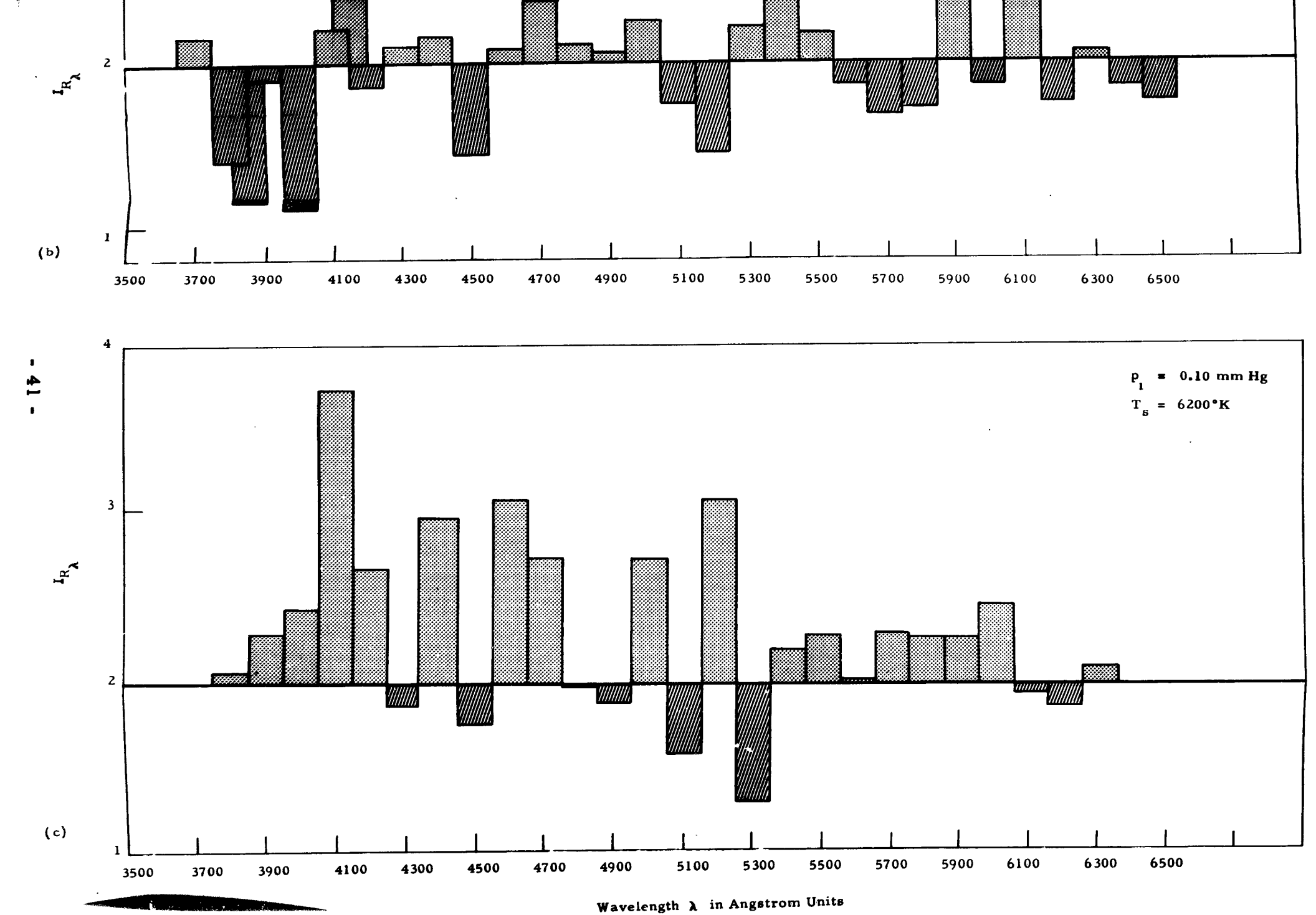

Fig. 12 AVERAGE SPECTRAL LIGHT INTENSITY RATIO $I_{R_\lambda} = \frac{\text{I - 3/4" dia. Model}}{\text{I - 3/8" dia. Model}}$

considerably more advanced nonequilibrium, since most of the data yield intensity ratios greater than the model scale. Likewise, at a particular wavelength, the chages in the radiation profile as a function of initial pressure can be deduced. Consider, for example, radiation flux and the intensity ratios at 4100 and 4500 A for 1, 0.15, and 0.1mm Hg pressures. Figures 13 and 14 depict the resulting situation. The nature of Figure 12 will be considered in greater detail in conjunction with the spectroscopic work which was carried out to learn the identities of predominant radiators.

4. Spectroscopic Studies

This investigation was made to identify the predominant air and impurity radiators in the bow shock layer. Two sets of spectrograms were obtained, one set was of light collected from the stagnation point, the other by transverse viewing across the shock tube through a quartz window. In the second case a quartz lens was used to image the bow shock region on the spectrograph entrance slit. The spectra were obtained using a Hilger E-517 quartz spectrograph. Preliminary work used Polaroid-3000 sheet film. Because of its high speed, a single exposure is sufficient to obtain a spectrogram even at densities corresponding to 0.1mm Hg pressure and flow times of 10 microseconds. The spectral response of Polaroid-3000 sheet film is comparable to F-103 spectrographic plate over a spectral region from 6500 to 2000 A. The resolution is poorer because of larger grain size; hence, positive identification of species characterized by a fine line structure is not always possible. Since the spectrograms obtained

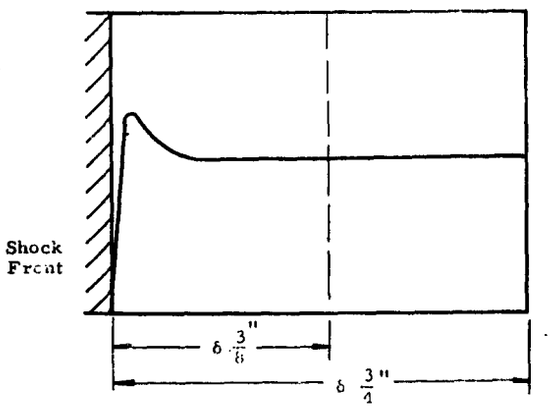

$\frac{I_{3/4}}{I_{3/8}} = 1.84$

1 mm Hg pressure

$T_s = 6200°K$

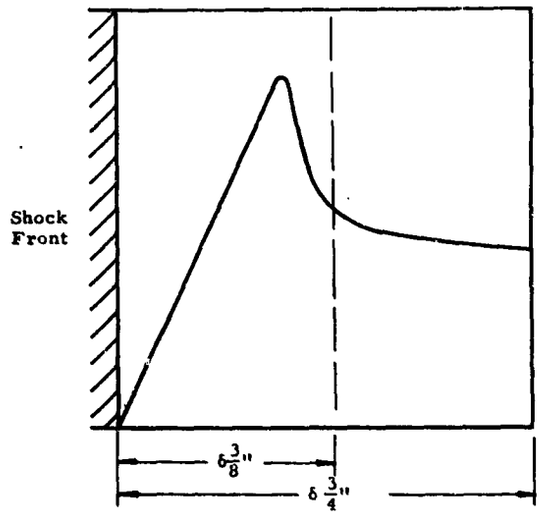

$\frac{I_{3/4"}}{I_{3/8"}} = 2.2$

0.15 mm Hg pressure

$T_s = 6200°K$

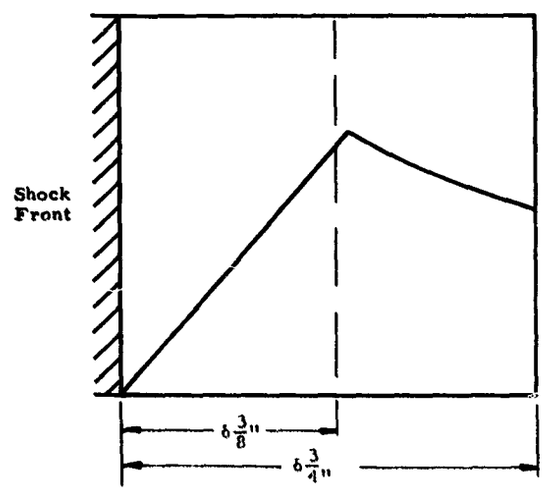

$\frac{I_{3/4"}}{I_{3/8"}} = 3.7$

0.1 mm Hg. pressure

$T_s = 6200°K$

Note: δ 3/8" and δ 3/4" are stand off distances for 3/8" and 3/4" diameter models respectively.

Fig. 13 RADIATION INTENSITY PROFILES λ = 4100 A

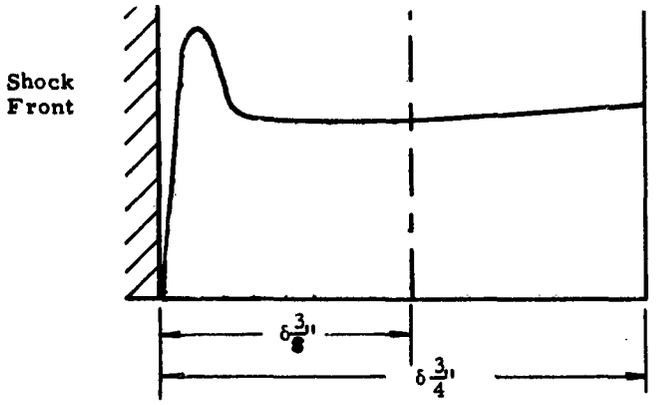

$\frac{I_{3/4"}}{I_{3/8"}} = 1.83$

1 mm Hg pressure

$T_s = 6200°K$

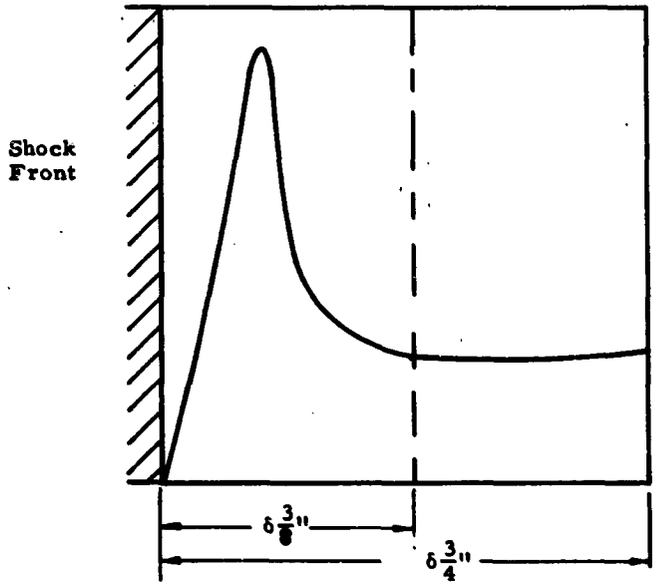

$\frac{I_{3/4"}}{I_{3/8"}} = 1.44$

0.15 mm Hg pressure

$T_s = 6200°K$

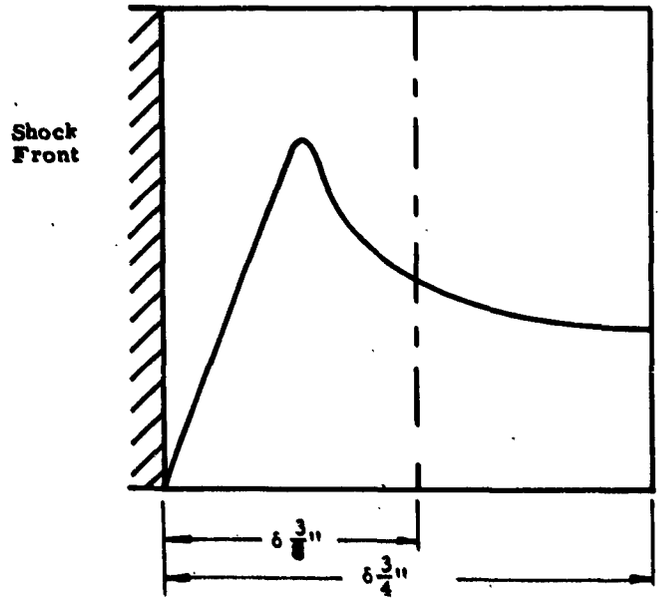

$\frac{I_{3/4"}}{I_{3/8"}} = 1.75$

0.1 mm Hg pressure

$T_s = 6200°K$

Note: δ 3/8" and δ 3/4" are stand off distances for 3/8" and 3/4" diameter models respectively.

Fig. 14 RADIATION INTENSITY PROFILES λ = 4500A

are positive paper prints, intensity measurements with a microdensitometer cannot be made. Attempts were made to rephotograph these prints and generate a transparency, which could be used for the analysis. This process is associated with some loss of detail and is applicable only in cases where clearly defined radiators are encountered. Such technique was used to evaluate the shock tube impurity radiation for various tube conditions. To obtain more positive identification of radiators, a number of spectrograms were obtained using 103-F spectrographic plates. Unfortunately, the exposures, even with many repeated runs, were not sufficiently good to yield adequate information about the radiators in the wavelength regions greater than 4500 A. This applies in particular to the low density flow regimes.

Spectrograms were obtained at ρ/ρ_0 ratios equal to 0.08, 0.015 and 0.008 corresponding to initial shock tube pressures of 1, 0.15 and 0.1mm Hg respectively. The shock tube was outgassed to 1 micron pressure with the associated leak rate of 10μ/ hour. The spectrograms were obtained by viewing through the stagnation point. The spectrograph slit was equipped with a fast shutter (closing time, approximately 20 microseconds) to avoid any exposure from the reflected shock.

General features of the spectrograms have been elucidated by taking microdensitometer traces and using a mercury spectrum for wavelength determinations. The following conclusions were made:

1. A general continuum exists which rises at around 2300 A and decays at around 5000 A. This wavelength range covers the NO-β system and it is fairly certain that the continuum is due to these broadened bands. In addition, there are probably contributions from the Schumann-Runge band and from the O^- continuum but these could not be identified.[21]

2. From air radiators, the NO-γ system was quite distinct, as was the N_2(1st positive). Small features between 4200 A and 5700 A are probably due to the N_2^+ (1st negative) system but these bands were not positively identified.

3. The radiators OH, CN and NH give very pronounced spectra.

- OH - $^2\Sigma \rightarrow {}^2\pi$ systems, the (0,0) band at 3064 A and the (1,0) band at 2811 A are very pronounced, showing much structural detail.
- CN violet bands are observed quite clearly at

3584 A	(3,2)
3586 A	(2,1)
3590 A	(1,0)
3883 A	(0,0)

and (1,1), (2,2), (3,3) collectively. The (0,1), (1,2) and (1,3) bands at 4216, 4197 and 4181 A respectively are observed superimposed upon other band radiations which, although not

positively identified, are thought to be CH.

- The NH system was observed at 3360 and 3371 A in the $^3\Sigma\ ^3\pi$ system. The compressed Q-branches of the (0,0) and (1,1) bands are very pronounced with the P and R branches on either side.

4. In the flow regimes corresponding to 0.15 and 0.1mm Hg at 4310 A there exists a very pronounced line or band (Figure 15). Wavelength determination was not sufficiently accurate to overrule this being 4315 A, which suggests the CH (0,0) band. Furthermore, to shorter wavelength there is another excursion at around 4160 A which could be an extension of this system. However, this is superimposed by the CN bands mentioned earlier, so the shape cannot be easily verified. To longer wavelengths, at 4390 A, another peak is observed but has not been identified. It corresponds to the position of C_2 Swan-band but other, stronger, bands of this system which should coexist were not observed. A test run was made in pure N_2 in an attempt to determine the origin of this radiation. Figure 16 shows the spectrogram that was taken. The radiation profile peaking at around 4120 is very strong and the CN band heads can be identified. However, this cannot all be due to CN because the (0,1) band at 4216 A should be the most intense. This feature appears in the spectrograms taken with air at the lower pressure but the overall intensity is much stronger with shocks

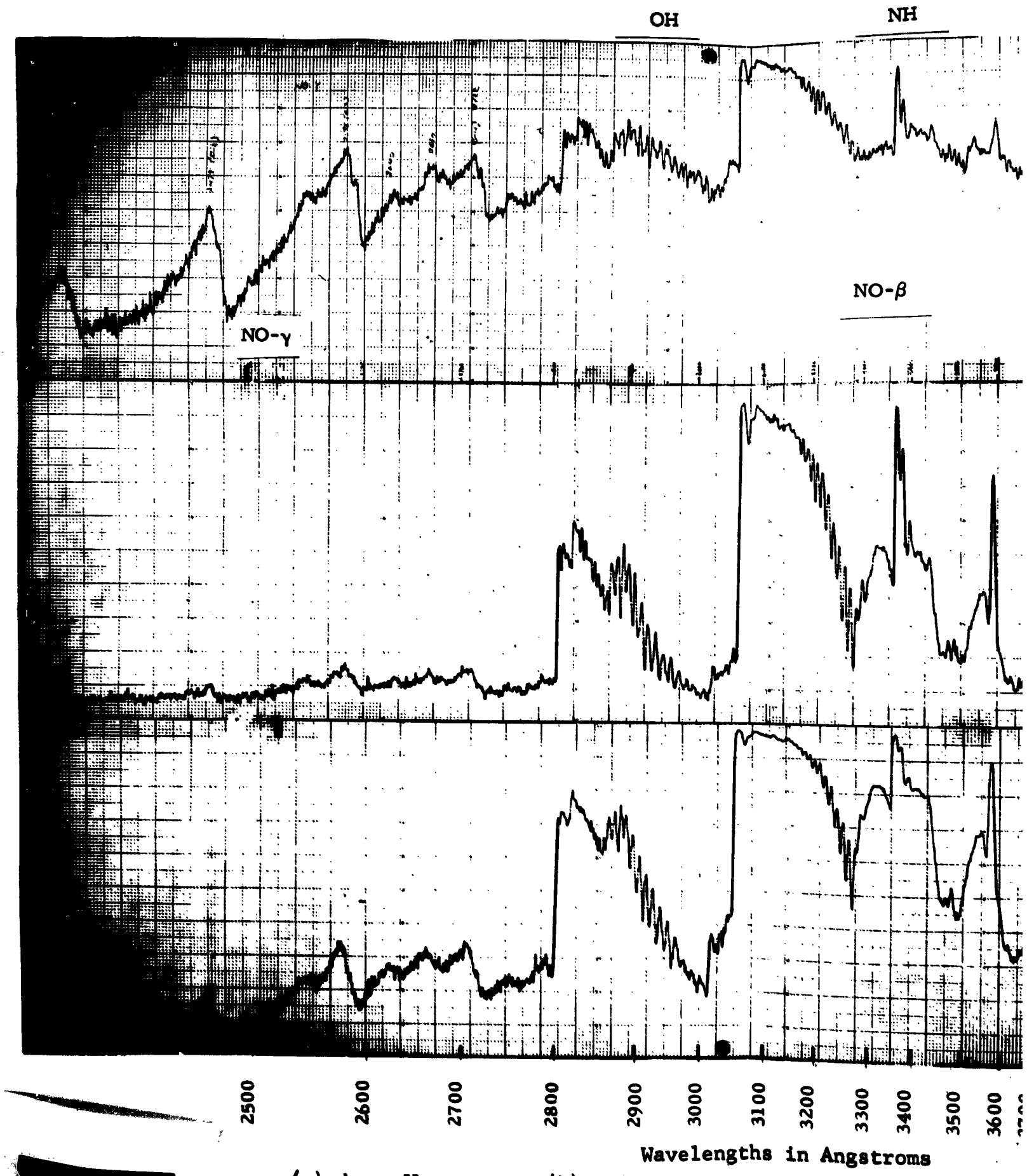

(a) 1 mm Hg pressure, (b) 0.15 mm Hg pressure, (c) 0.10 mm Hg

Fig. 15 MICRODENSITOMETER TRACES, FROM SPECTROGRAMS THROUGH THE STAGNATION POINT

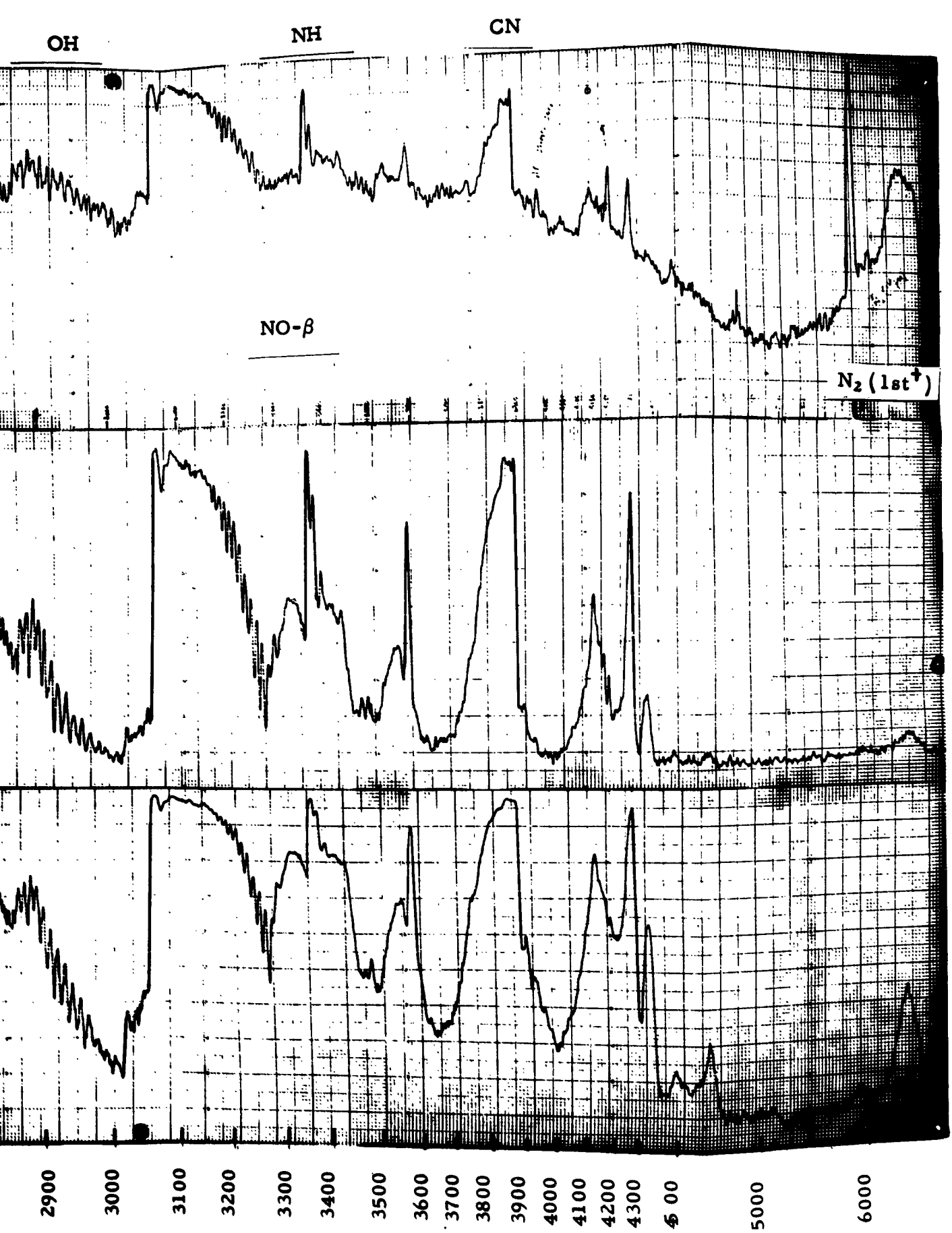

0.15 mm Hg pressure, (c) 0.10 mm Hg pressure, at T_s = 6200°K

METER TRACES, FROM SPECTROGRAMS OBTAINED BY VIEWING STAGNATION POINT

12

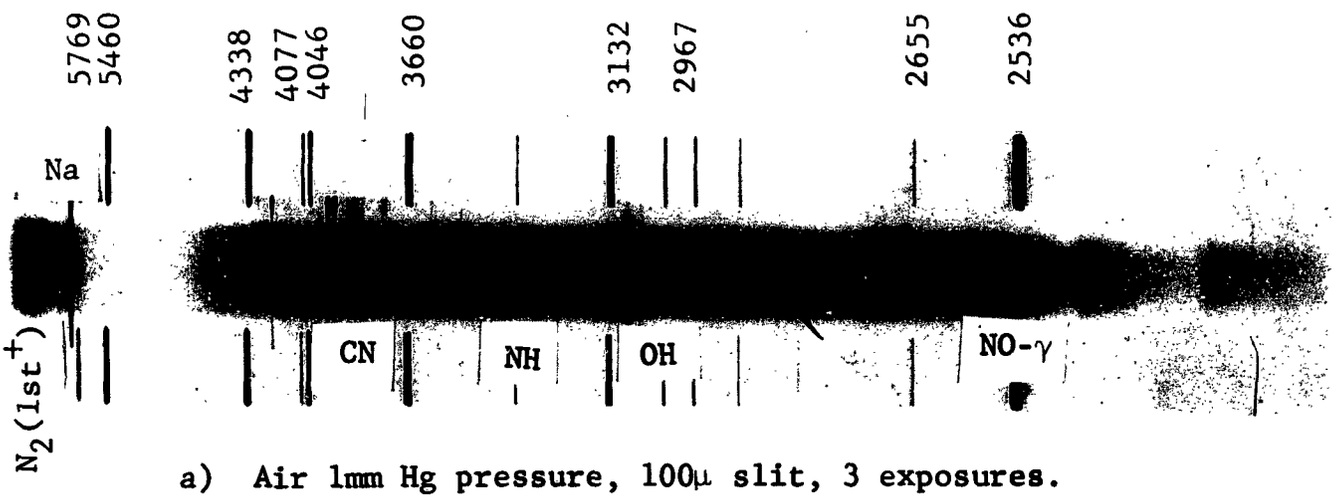

a) Air 1mm Hg pressure, 100μ slit, 3 exposures.

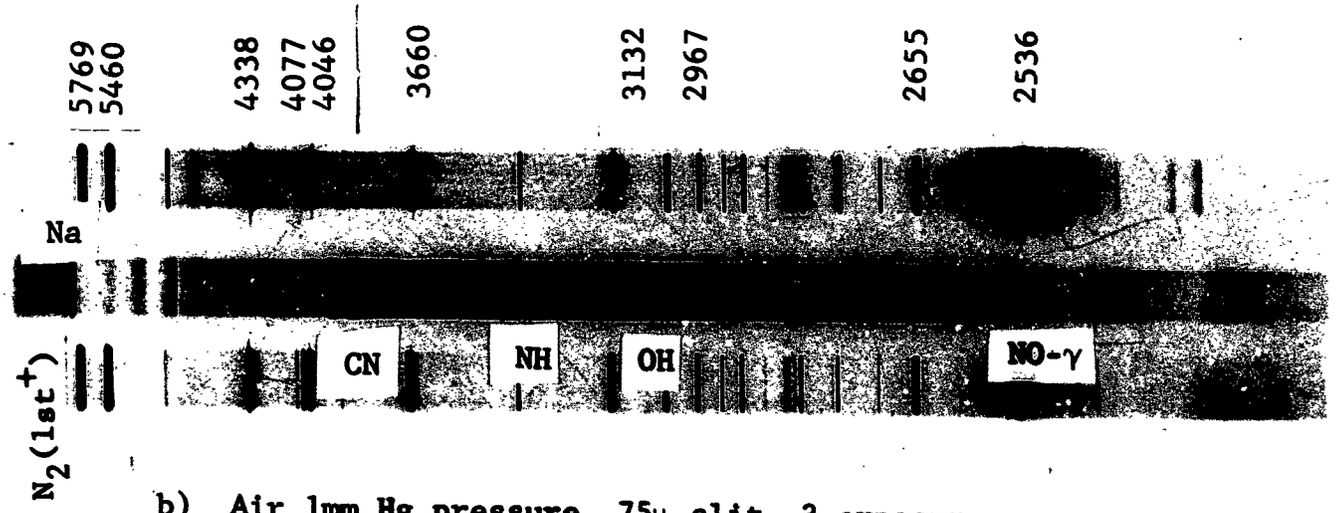

b) Air 1mm Hg pressure, 75μ slit, 3 exposures.

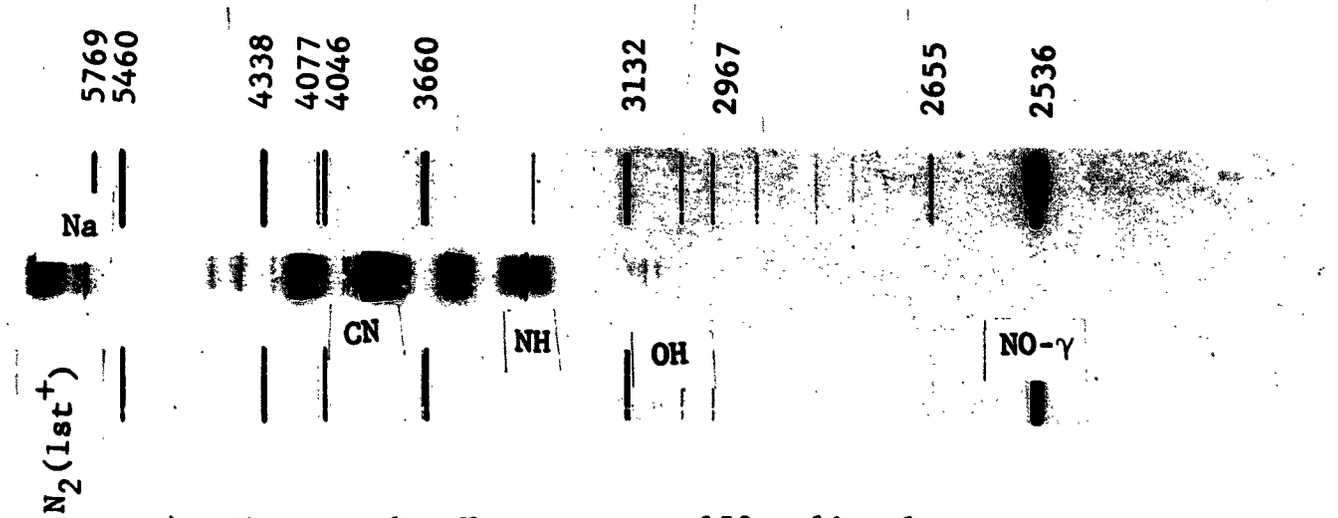

c) Nitrogen 1mm Hg pressure, 150μ slit, 1 exposure.

Fig. 16 SPECTROGRAMS OBTAINED BY TRANSVERSE VIEWING

in pure N_2. Hence it appears that the radiator is nitrogen or a nitrogen compound with CN violet bands superimposed. The intensity of this radiation is such that it could not be entirely due to the N_2 (2nd positive) or N_2^+ (1st negative) systems since other bands of these species were weak.

5. At 1mm Hg pressure these features were not seen; instead, two distinct lines, 4210 and 4300 A, were evident, Figure 15a. The lines at 4210 and 4300 A have the appearance of atomic lines but have not been positively identified because of inaccuracies in wavelengths. The Na doublet, unresolved, at 5890 A is also observed very strongly.

In general, the continuum and positively identified normal air radiators were most pronounced at high pressure. At low pressures the Na doublet was not observed nor were the two lines at 4210, 4300 (Figure 15a) leading us to believe that they had a similar origin to the Na and were atomic lines. Similarly, the feature arbitrarily ascribed to CH at 4315 A (to shorter wavelength) appears at low pressure, thus encouraging the belief that the radiation is from a gas radical.

The decrease in intensity of the background with decreasing density is expected. Not only is the total gas density decreased but also the equilibrium concentration of NO falls by a factor of 30 when the pressure changes by a factor of 10. However, the intensity of the gas radical emissions does not decrease in the same way. This results in an increased

importance of this type of emission at the lower pressure and, since these radicals are notorious transient emitters behind shock waves, nonequilibrium radiation can be expected to play an increasing part as the pressure is reduced because the relaxation processes are becoming slower. We can also expect nonequilibrium effects from air components. Such radiators have been observed by various workers[1, 2, 3, 4, 5, 18] with NO, N_2^+ (1st positive), these being a sharp radiation overshoot immediately behind the shock front.

At this point, it is appropriate to compare the microdensitometer trace (Figure 15) with the photomultiplier data (Figure 9) and the intensity ratios given in Figure 12. Figure 9 shows especially high emission at 3900 and 4200 A which, as the spectrogram shows, is due to CN emission. Figure 12 shows a different state of affairs. The regions of maximum emissions are not the only ones which do not scale and therefore, by implication, show the effect of nonequilibrium. As expected, the greatest departure from equilibrium occurs at the lower pressures.

As the pressure is decreased, there is appreciable nonequilibrium indication. We can define two categories of departure from equilibrium:

(1) fast, in which the scale factor is less than two, and

(2) slow, in which the scale factor is greater greater than two

and using these descriptions, some of the features can be correlated with the spectrograms and microdensitometer traces.

Fast. At 1mm Hg pressure, the most pronounced fast radiators are Na line and CN radiation (Figure 12a). Such radiation characteristics are easily understood, since Na radiation is unchanged, i.e., it originates on the model surface and in such a case does not depend on model scale. Likewise, CN is a notable transient radiator and may originate on the body surface as well as from the contaminants in the shock front. In general, with the exception of few radiators, as discussed previously, the nonequilibrium radiation is expected to be so fast as to be undetectable at higher pressures and to slow down as pressures are decreased. Hence, the fast regime is expected first. This means that constituents other than CN are too fast to be observed.

As pressure is decreased to 0.15 mm Hg (Figure 12b) there is much more variation, more of the fast and more of the slow regimes. In particular, the regimes around 4000, 4500, and 5200 A are fast and do not correspond to any readily identified features such as CN, OH and NH. This means that the background radiation is now fast but not sufficiently fast that its effect cannot be noticed -- it is slowing down. This is consistent with observations and calculations on NO-β and NO-γ radiations by a number of authors. In this case the NO-β is probably the cause.

When the pressure is decreased to 0.1mm Hg, as Figure 12c shows, most of the radiation is slow. In particular, the regimes mentioned, namely 4000, 4500, and 5200 A are either slow or less fast than before, showing that non-equilibrium processes are indeed taking place. At 5300 A the radiation is faster than most because it is lagging behind the rest in moving through the fast to the slow stage. This implies that there is a very efficient excitation process at this wavelength.

Slow. It is difficult to see why isolated spectral regimes are slow unless the radiations are not normal air components, e.g., dust taken off the shock tube walls. While some of the slow regimes shown for 1mm Hg pressure may be due to experimental error, that at 6100 A seems too large. The N_2 (1st positive) systems start around this wavelength but it is strange that only part of this region is slow and that at higher wavelengths the radiation is fast. This discrepancy is quite pronounced at 0.15mm Hg pressure; in fact, the sequence in Figure 12 suggests that there is a component at this wavelength region which becomes steadily slower until at 0.10mm Hg it is no longer a significant radiator and at this pressure a weaker radiator, a fast one, predominates. The suggestion is that the radiation line is not just N_2 (1st positive) but could include C_2 Swan, for example.

The block diagram for 0.15mm Hg pressure presents an interesting study. It shows both slow and fast regimes with

the transition toward the slow (compare with 0.10mm Hg). The figure implies that different species dominate in the different regions. If we postulate that the background (probably NO-β predominantly) is slow and that, at certain points, other fast radiation dominates, then:

at 4150 A lies the ambiguous radiation ascribed tentatively to CH overlaid by CN. This is very slow, but at 4200 A the net result is fast. Thus, CN is fast (see also 3850 A) and so is another radiator at 4000 A.

at 4500 A a fast radiator exists which could be N_2^+ (1st negative) with the following bands:

4600 A	(2,4)
4554 A	(3,5)
4518 A	(4,6)

at 5100 to 5200 A fast radiators are present. Here the relevant N_2^+ (1st negative) bands are:

5076	(2,5)
5148	(1,4)
5228	(0,3)

at 6000 A radiators are fast (except for 6100 A). This is the region of N_2 (1st positive) radiation.

The N_2^+ (1st negative) bands listed are the strongest in this region which is quite consistent with the idea that these bands contribute more than the NO-β bands at specific spectral regions for the detection band width of 100 A.

Finally, the data for pressure of 0.10mm Hg pressure show that most systems are now slow. However, certain regions, such as 5300 A, 5100 A and 4900 A are now faster than before. This means that in reducing pressure the slow component (NO-β) becomes less important than the fast. Such behavior is consistent with equilibrium calculations [23] showing a depletion of NO greater than that caused by the pressure reduction and a similar effect might be expected for the non-equilibrium regime. It is probable that this is not the whole answer because at 5700 A the radiation has become slow although this could be due to the N_2 (1st positive) system. It seems likely, therefore, that because of the decrease in pressure, not only is the NO-β system radiating less but also the bands are not so broad, introducing a further change in the radiation structure.

The overall features of Figure 12 have been correlated with the microdensitometer traces (Figure 15) of the spectrograms (Figure 17).

The results show that the change in radiation time histories of radiators emitting in excess of their equilibrium amount can be followed. It was also shown that the molecules whose nonequilibrium radiation could be detected or deduced relaxed in the following order, the first being the slowest: NO-β, CN-violet, N_2 (1st positive), N_2^+ (1st negative).

As mentioned, studies were also performed to ascertain the importance of shock-tube clean-up technique. A typical spectrogram showing additional impurities is shown in Figure 16. This spectrogram was obtained viewing the bow shock transversely. The shock-tube walls were not cleaned after the previous run. Spectrograms were also obtained when the tube was cleaned with ethanol but shock runs were made without sufficient outgassing. Under such conditions, the following shock-tube impurity radiators were disclosed:

AlO degraded to longer wavelengths

5079.3 (0,1)

4842.1 (0,0)

4648.2 (1,0)

C_2-Swan bands degraded to shorter wavelengths

5635.5 (0,1)

5585.5 (1,2)

5765.2 (0,0)

4737,1 (1,0)

4371.4 (3,1)

CH open structure visible in some spectrograms

4312.5 (0,0)

Comparison between spectrograms obtained by transverse viewing of the bow shock region (Figure 16) and by viewing through the stagnation point (Figure 17) indicates that the impurity radiation (in particular, CN) is not confined to the shock-tube boundary layer. However, it was not established

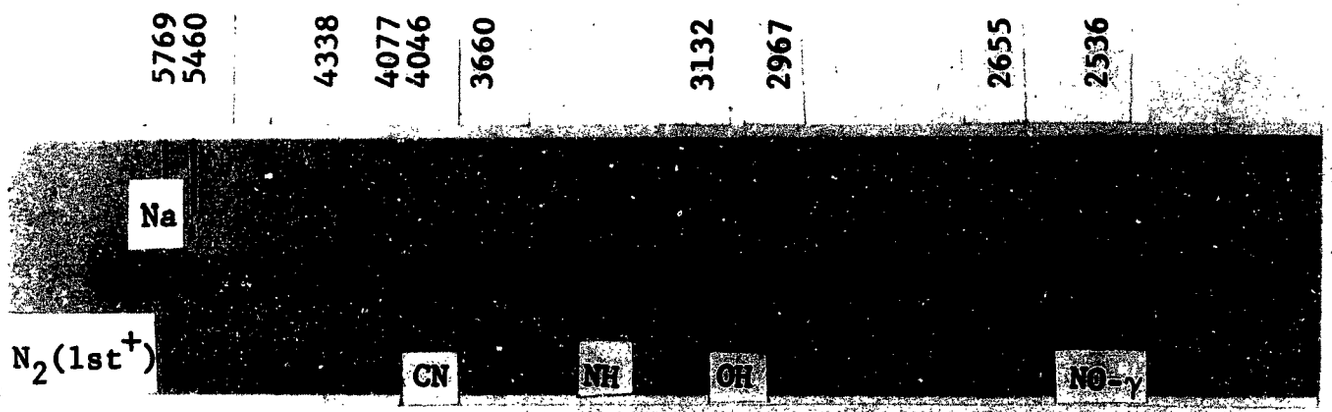

a) 1mm Hg pressure, 150μ slit, 17 exposures

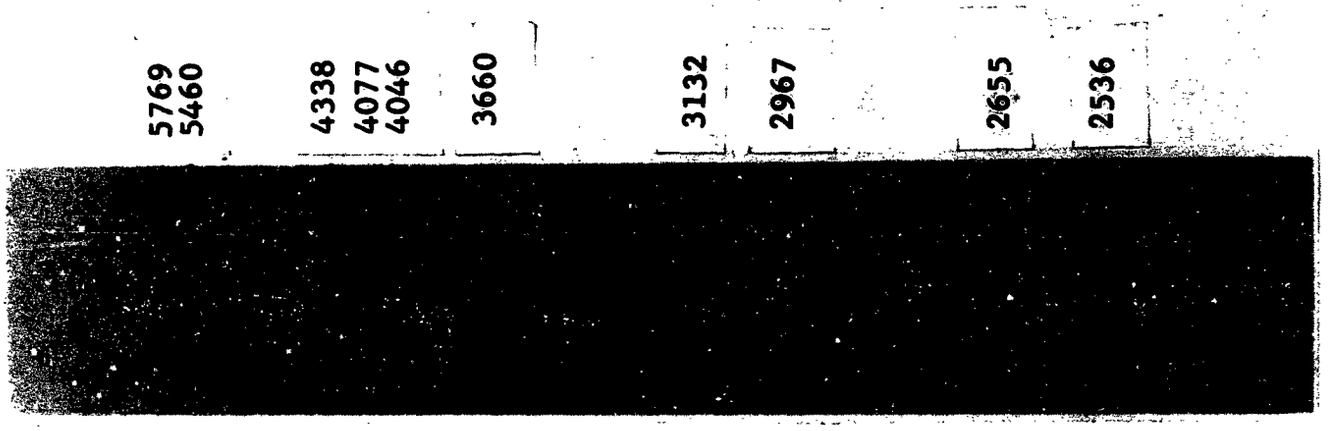

b) 0.15mm Hg pressure, 100μ slit, 12 exposures

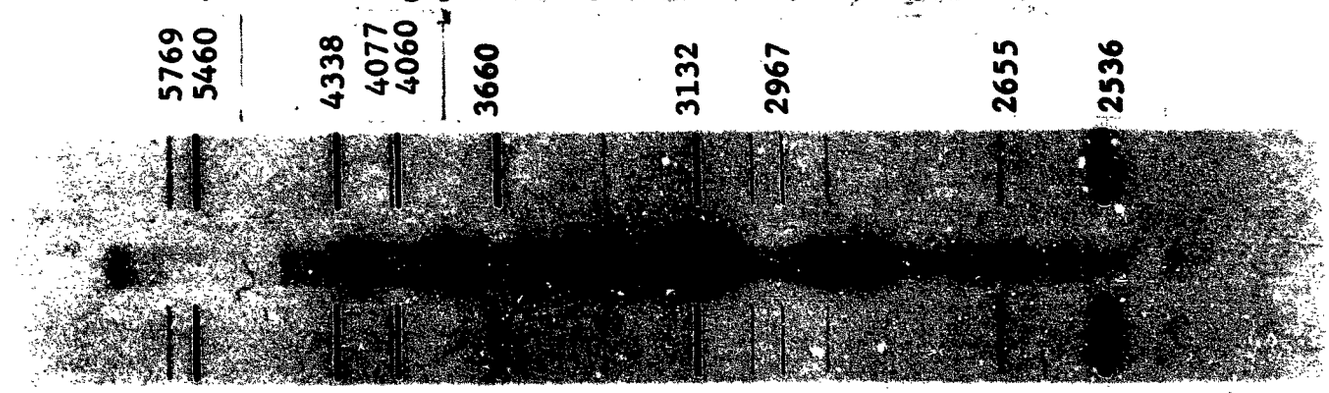

c) 0.1mm Hg pressure, 100μ slit, 8 exposures

Fig. 17 SPECTROGRAMS OBTAINED BY VIEWING THROUGH THE STAGNATION POINT

whether the CN radiation observed through the stagnation point is due to impurities on the model surface or to contaminants in the free stream. Further study is required to answer this question. In general, as shown in Figure 17, the spectrum obtained through the stagnation point is of a better quality and more details can be observed.

5. General Comments

To illustrate the quality of photomultiplier output from which light intensity was obtained, typical oscilloscope traces are shown in Figures 18 and 19. The output is essentially constant for the entire duration of luminosity, hence, the assessment of signal amplitude presents no problem. Exceptions were encountered at isolated spectral regions where impurity radiation predominates. For example, such is the trace in Figure 19a which shows transient behavior characterized by a fast nonequilibrium radiator such as CN.

Signals obtained at 5900 A (Figure 19b) show erratic behavior. This substantiates the conclusion that Na radiation stems from ablation of the glass window. Only in this portion of the spectrum (5800 - 5900 A) was pronounced radiation observed after the initial flow duration. The trace in Figure 19b for 200 microseconds per centimeter shows that 50 microseconds after the initial flow duration, a second radiative period takes place which lasts for approximately 100 microseconds. This probably corresponds to the arrival of the contact surface and the hot buffer gas. The arrival of the driver gas, approximately 800 microseconds later also causes

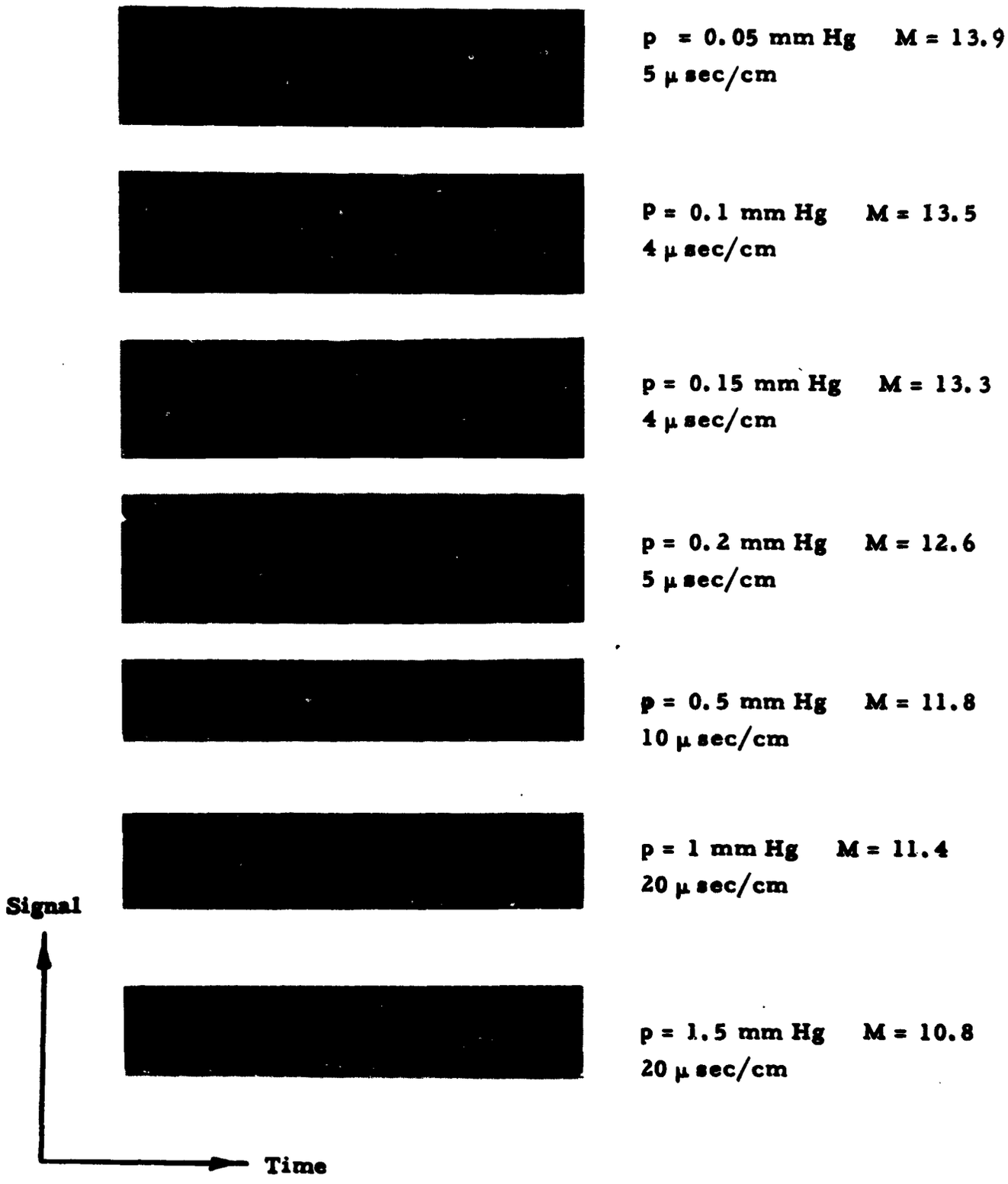

Fig. 18 LIGHT OUTPUT TRACES USING FIBER BUNDLE AS A LIGHT TUBE AT VARIOUS FLOW CONDITIONS

N6011

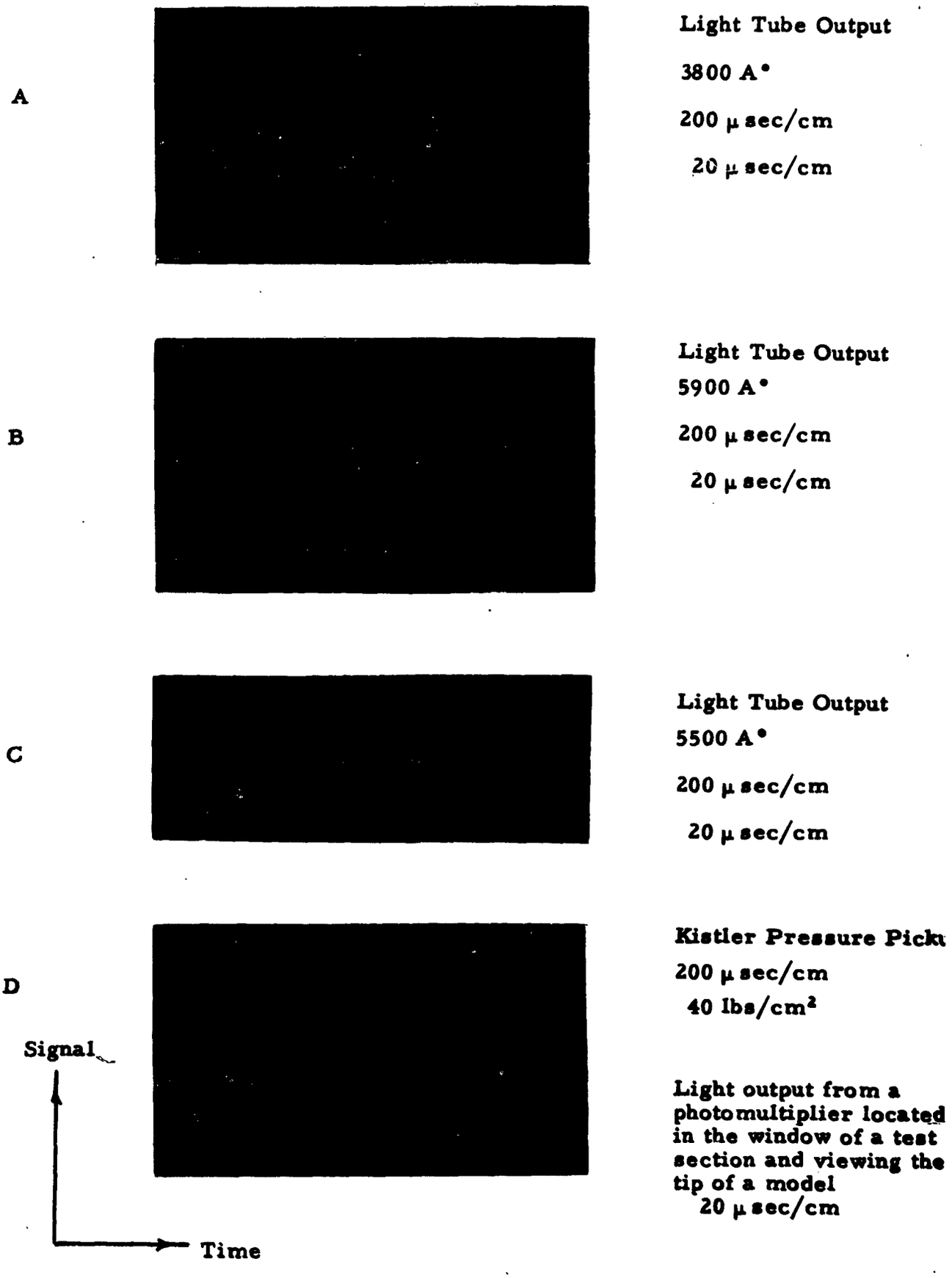

Fig. 19 TRACES SHOWING FLOW CHARACTERISTICS IN A SHOCK TUBE FLOW AT 1 MM HG PRESSURE AND M = 11.4

a small amount of light emission. To determine the pressure history associated with this flow regime, some measurements were performed with Kistler pressure pick-ups mounted in the test section. A pressure record, together with a photomultiplier output obtained through a side wall window in the test section, are shown in Figure 19d. The pressure remains essentially constant for about 160 microseconds, a period which is approximately twice the persistence of luminosity observed by the light tube. For the following 280 microseconds, the pressure rises only slightly, then there is a sudden increase followed by a gradual increase to 250 psia. The sudden jump occurs when the reflected shock wave passes the pressure sensor. It is interesting to note that the arrival of the reflected shock is seen by the side wall photomultiplier (lower trace Figure 19d) but is not seen by the light tube (Figure 19c). The gradual increase in pressure observed after 500 microseconds indicates the arrival of the helium driver gas.

The preceding discussion was included to emphasize that the constant-intensity portions of the light tube traces shown in Figure 18 do indeed correspond to conditions of steady flow of the test gas alone, rather than to a confused region of test, buffer, and possibly driver gas. The duration of luminosity has been correlated with the flow duration times given by Roshko[14]. The results are shown in Figure 20.

To evaluate the importance of outgassing pressure on impurity radiation, a series of test runs was made at 3900 A and 0.15mm Hg pressure using identical shock-tube

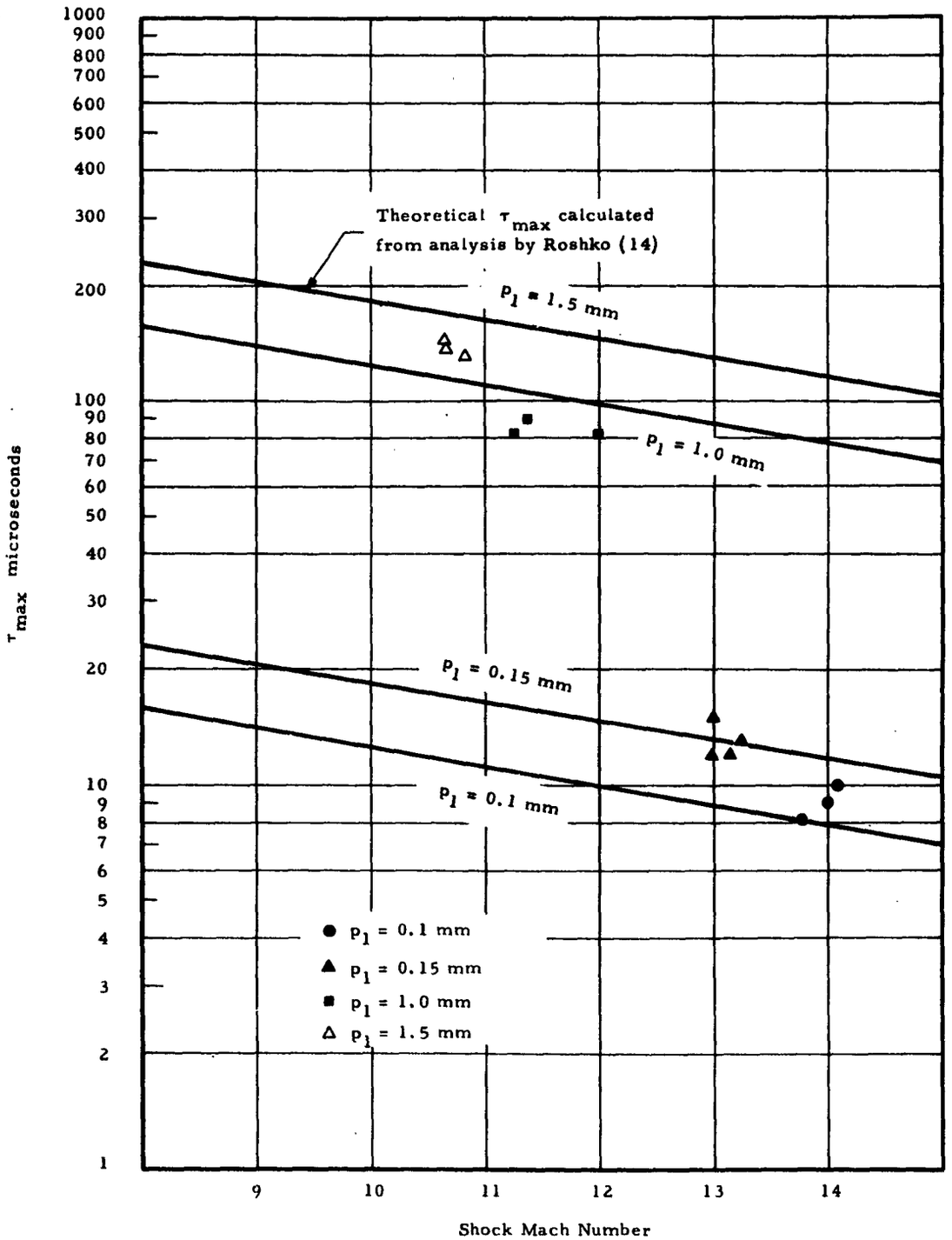

Fig. 20 DURATION OF LUMINOUS BOW SHOCK REGION

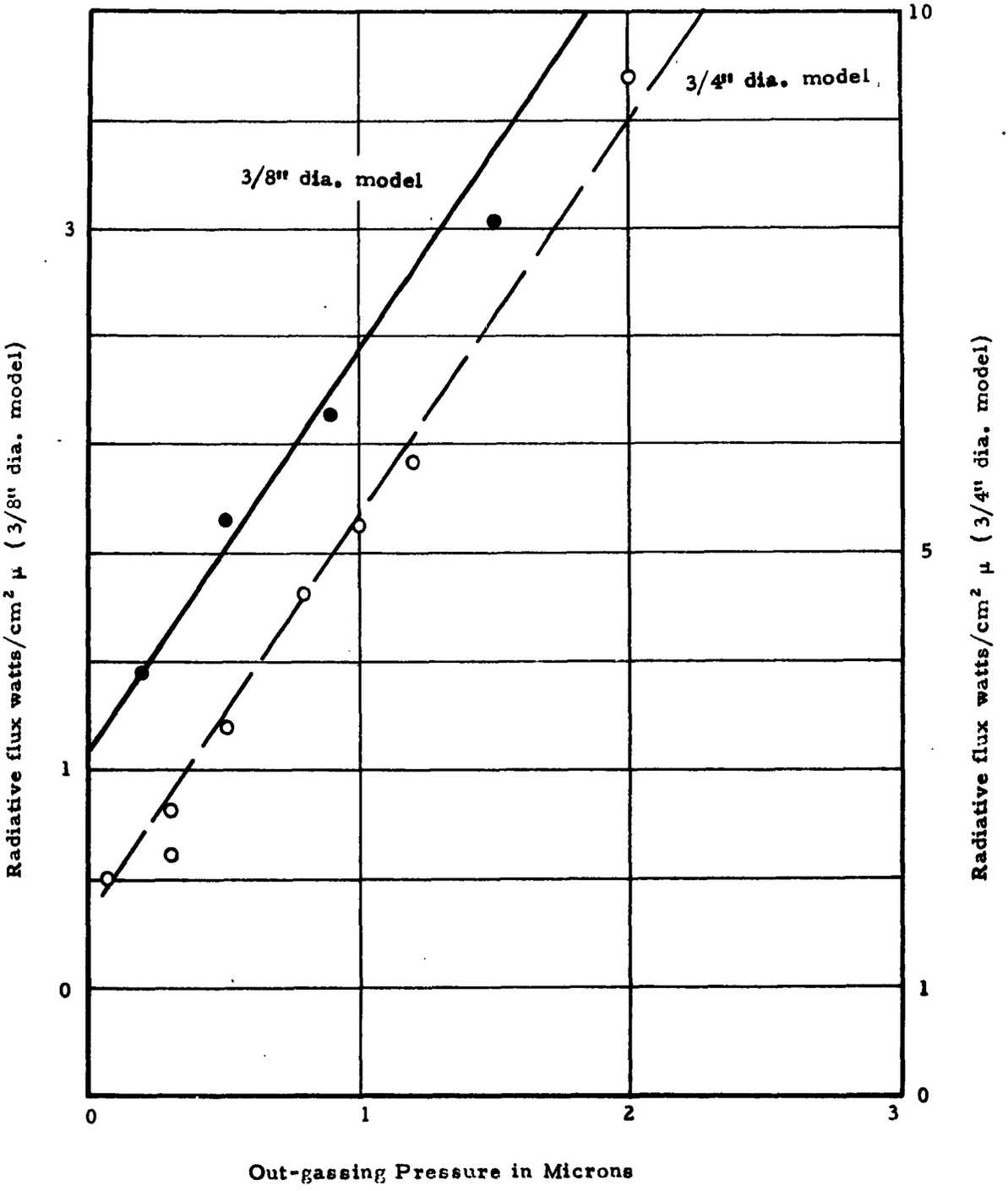

Fig. 21 THE EFFECTS OF SHOCK TUBE OUTGASSING PRESSURE ON THE RADIANT FLUX INTENSITY AT $\lambda = 3900A^0$

cleansing processes, but varying the outgassing pressure. The results are shown in Figure 21.

It is evident that, even after careful cleaning and flushing procedures, by changing the tube outgassing pressure from 0.1 to 2 microns, the radiant flux intensity increases by a factor of approximately four. Because the lowest values were reached by continuous outgassing in excess of 18 hours pumping time, such experimental procedures are not practical. The data shown in Figure21 include points obtained with outgassing pressures not greater than 1 micron. Similar data dependency on outgassing pressure was noted to a lesser extent at 4100 to 4300 A band widths. Again, this is responsible, at least in part, for data scatter in these spectral regions.

IV. CONCLUSION

The following conclusions are made from the several aspects of this investigation.

The radiant intensity measurements at the stagnation point of hemisphere-cylinders yield radiant flux values whick are less than 0.1 per cent of the aerodynamic heating experienced on the models of comparable scale, i.e., with mose radii from 0.5 to 1 cm. Consequently, large deviations from theoretical values in convective heat transfer measurements[20] cannot be attributed to excessive radiative flux.

Measurements made with two models of different characteristic dimensions substantiate scaling arguments as criteria for the extent of flow nonequilibrium. Consequently, a technique

is developed which enables experimental determination of flow regimes in the shock tube and shock tunnel flows for which model test results can be scaled for the evaluation of radiant heat flux during reentry. These criteria applied to the current problem indicate that, for a stagnation temperature of 6200°K, an initial pressure of 0.3mm Hg constitutes the lower limit. Tests performed at lower pressures indicate pronounced nonequilibrium effects.

Spectrographic investigation shows that the predominant air radiators are NO-β, NO-γ, N_2 (1st positive). Positive identification of N_2^+ (1st negative) and oxygen (Schuman-Runge) was not possible. The investigation also disclosed that, despite very careful shock tube preparation, even stagnation point measurements show quite strong impurity radiation. The most important identified radiators are CN, OH, and NH and at higher densities, unresolved Na doublet was observed. The fact that data were obtained viewing the luminous region through the stagnation point, indicates that impurity radiation is not generated solely in the shock tube boundary layer flow. Pronounced radiation of the latter type was observed only in cases where shock tube walls were not cleaned between the successive views. In such cases, AlO and C_2 bands were observed as very strong radiators in the visible portion of the spectrum. Lowering initial shock tube pressure results in a considerable increase in the impurity radiation and contributes to the nonequilibrium effects.

Radiant intensity measurements at 1mm Hg pressure and 6200°K compare favorably with equilibrium values calculated by Breene et al,[21] except at wavelengths where impurity radiation dominates. On the other hand, measurements at 0.1mm Hg pressure show large departures from the theoretical equilibrium predictions. This factor again indicates nonequilibrium flow and substantiates the scaling arguments discussed here.

This work shows that light tube techniques can yield useful data on radiation to the stagnation point behind the bow shock which would be difficult to calculate without making grave assumptions.

REFERENCES

1. Wray, K., et al, "Relaxation Processes and Reaction Rates Behind Shock Fronts in Air and Component Gases," AVCO R-83, Dec., 1959.

2. Camac, M., J. Keck, and C. Petty, "Relaxation Phenomena in Air Between 3000 and 8000°K", AVCO R-22, March 13, 1958.

3. Allen, R.A., J. Keck, and J.C. Camm, "Non-Equilibrium Radiation from Shock Heated Nitrogen and Determination of theRecombination Rate," AVCO R-110, June, 1961.

4. Hammerling, P., J.D. Teare, and B. Kivel,"Theory of Radiation from Luminous Shock Waves in Nitrogen," AVCO R-49, June, 1959.

5. Kivel, B., "Ionization and Radiation in the Non-Equilibrium Front of Normal Shocks in Air," AVCO AMP-34, September, 1959.

6. Herzberg, A., Russo, A.L., "Modifications of Basic Shock Tube", CAL Report 58716 (1958).

7. DeVos, J., Physika, vol. 20, pp. 690-714, 1954.

8. IITRI Project 4252, Final Report, March 19, 1962.

9. Inger, G.R., "Viscous and Inviscid Stagnation Flow in a Dissociated Hypervelocity Free Stream", Aerospace Corp. Report TDR 62-143 (1962).

10. "Gaseous Radiation in Hypersonic Stagnation Point Flow", IITRI Project N 6011 Semi-Annual Report, January 15, 1963.

11. Feldman (tables), "Hypersonic Gas Dynamic Charts for Equilibrium Air", AVCO Research Lab, 1957.

12. Van Dyke, M., J. Aero/Space Sci. 25, 485-496 (1958).

13. Serbin, H., J. Aero Sci. Readers' Forum, 25, 58 - 59(1958).

14. Roshko, A., Physics of Fluids 3, 835-842 (1960).

15. Hacker, D.S. and L.N. Wilson, Conf. on Manned Re-entry AFOSR, Philadelphia, November, 1962.

16. Burke, A.F., J.T. Curtis and D.W. Boyer, "None-Equilibrium Flow Considerations in a Hypervelocity Wind Tunnel", CAL Report AA 1632-Y-1 (1962).

17. Hayes, W.R., Probstein, R.F., Hypersonic Flow Theory, Academic Press, 1959.

18. Camm, J.C., Kivel, B., Taylor, R.L., Teare, J.D., "Absolute Intensity of Non-Equilibrium Radiation in Air and Stagnation Heating at High Altitudes", J. Quant. Spect. Radiat. Transf. 1, 53, September, 1961.

19. Hall, J.G., Eschenroeder, A.Q., Dismore, P.V., "Initial Hypersonic Arc-Flows in the Completed Non-Equilibrium Pressure", IAS 30th Annual Meeting, N.Y., January 22-24, 1962, paper # 62-67.

20. Rutkowski, R.W., "A Note Regarding Stagnation Point Radiation" Report LMSD 288139, January, 1960.

21. Breene, R.G., Hardone, M.C., "Radiant Emission from High Temp. Air", J. Quant. Spect. Rad. Transf. 2, 273, 1962.

22. Kivel, B., Bailey, K., AVCO Res. Rept. 21, 1957.

23. Gilmore, F.R., "Equilibrium Composition and Thermodynamic Properties of Air to 24,000°K", The Rand Corp. RM-1543, 24 August, 1955.